The Thesis Committee for Runqi Han
Certifies that this is the approved version of the following thesis:

AUTOMATED COMPUTER VISION SYSTEM FOR REAL-TIME DRILLING CUTTINGS MONITORING

APPROVED BY

SUPERVISING COMMITTEE:

Supervisor:

Eric van Oort

Mitch Pryor

Pradeepkumar Ashok

AUTOMATED COMPUTER VISION SYSTEM FOR REAL-TIME DRILLING CUTTINGS MONITORING

by

Runqi Han, B.S.

Thesis

Presented to the Faculty of the Graduate School of

The University of Texas at Austin

in Partial Fulfillment

of the Requirements

for the Degree of

Master of Science in Engineering

The University of Texas at Austin

August 2016

Dedication

To my parents and girlfriend，   for their endless love and support.

Acknowledgements

Abstract

AUTOMATED COMPUTER VISION SYSTEM FOR REAL-TIME DRILLING CUTTINGS MONITORING

Runqi Han, M.S.E

The University of Texas at Austin, 2016

Supervisor: Eric van Oort

In rotary drilling operations, cuttings are continuously transported to the surface by drilling fluid. Real-time monitoring of cuttings and cavings is crucial for early detection and remediation of drilling problems such as stuck pipe, lost circulation, high torque and drag, reduction in rate of penetration, and other wellbore instability issues. These incidents are large contributors to drilling-related Non-Productive Time (NPT). At the current stage, a mud logger performs monitoring manually. This work proposes to use computer vision techniques to automate this procedure. To achieve this application, specific requirements should be established to design an automated machine vision system to maintain drilling safety and speed.

Cuttings ramp has been identified as an ideal location to perform the measurement, where cuttings and caving are sliding down a slope at a steady speed. To accomplish this task, an intelligent image processing system must be able to track cuttings speed, measure volume, analyze size, and generate a surface model. Through a detailed review and testing of available 3D sensing techniques, a system consisting of a 2D high-resolution camera

and 3D laser profile scanner was designed. By implementing image processing techniques, the cuttings speed on the ramp was estimated which was then synchronized to the 3D depth data from a laser scanner. Finally, the volume of moving cuttings was estimated and a 3D surface profile was reconstructed using point cloud data.

Experimental results in the lab environment validated that such a system can be applied to quantify cuttings volume, size distribution, and reconstruct a 3D profile of cuttings and cavings. This measured result can be stored for further analysis. Overall, this work established a foundation for the design of a sophisticated real-time monitoring system for hole cleaning and wellbore risk reduction.

Table of Contents

List of Tables

List of Figures

Chapter 1: Introduction

1.1 MOTIVATION AND OBJECTIVES

In oil and gas well drilling, one of the key drilling processes is to transport drilled debris (drilling cuttings) to the surface via drilling fluid. Drilling cuttings and fluid are then separated by a shale shaker system as shown in Figure 1-1. Inefficient cuttings transport may result in poor hole cleaning problems. Hole cleaning remains a big challenge in both directional and vertical wells. Poor hole cleaning can lead to a series of costly drilling inefficiencies such as: mechanical pipe sticking, excessive torque and drag on drill string, slower rate of penetration, bottom hole assembly damage, poor cement job, etc. (O.C.T.G. Procter Consultancy Ltd 2000). Incidents like wellbore instabilities and stuck pipe can lead to a halt in drilling operations for days and burn through millions of dollars (C. Aldea 2005). All these problems may severely jeopardize the safety of drilling personnel on a rig.
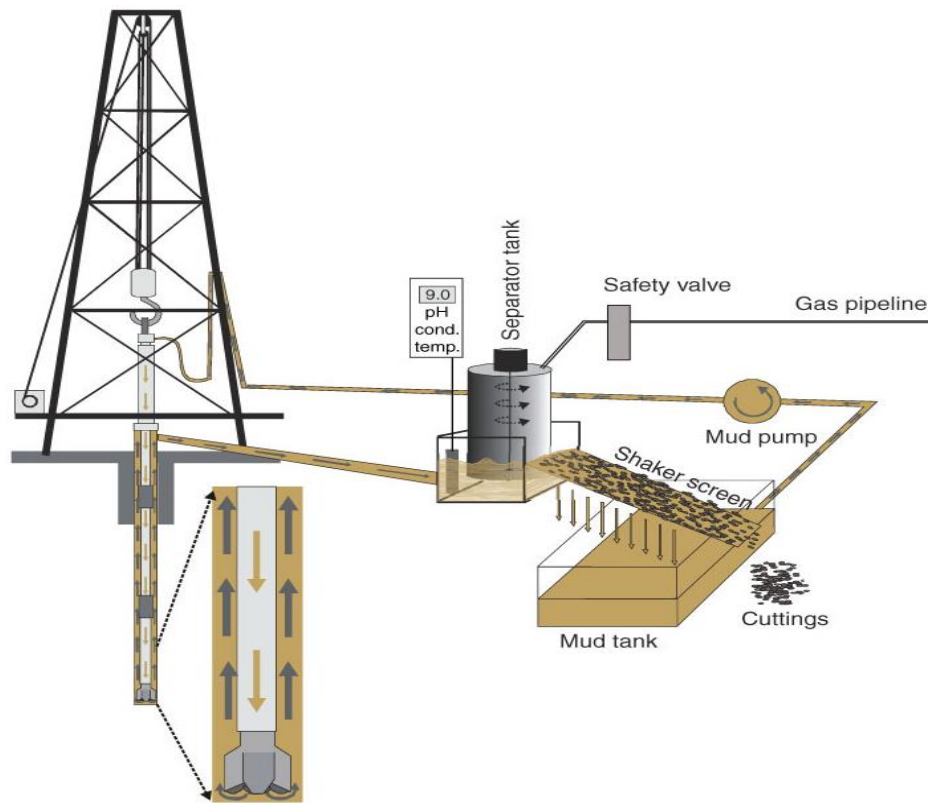
Figure 1-1: Schematic illustration of drilling process (Wiersberg 2009)

Monitoring return cuttings provides a direct assessment of hole cleaning efficiency. As shown in Figure 1-2, one of the traditional methods to assess the efficiency of cuttings recovery is by assigning a mud logger to continuously monitor cuttings on a shale shaker system (Morton-Thompson and Woods 1993). A mud logger creates a detailed record of wellbore formation and condition. The mud logging report (as shown in Figure 1-2) contains drilling cuttings properties and drilling fluid conditions. The physical lithological data of downhole formation can be recovered by analyzing collected cuttings and cavings samples with regard to their physical appearances. However, this is a tedious and labor-intense process and it lacks a thorough and structured approach. Cuttings return volume also cannot be measured based on a visual check from the mud logger. In addition, a mud

logger is continuously exposed to high hydrocarbon mist and vapor at the shale shaker house. Because of the routine duties like: washing with high-pressure guns using hydrocarbon-based fluid, collecting cuttings, and measuring drilling mud, workers' health and safety is threated both by inhaling toxic vapors and by direct skin contact (IPIECA 2009). Therefore, automating this process will be very beneficial to the drilling operations and personnel health and safety.
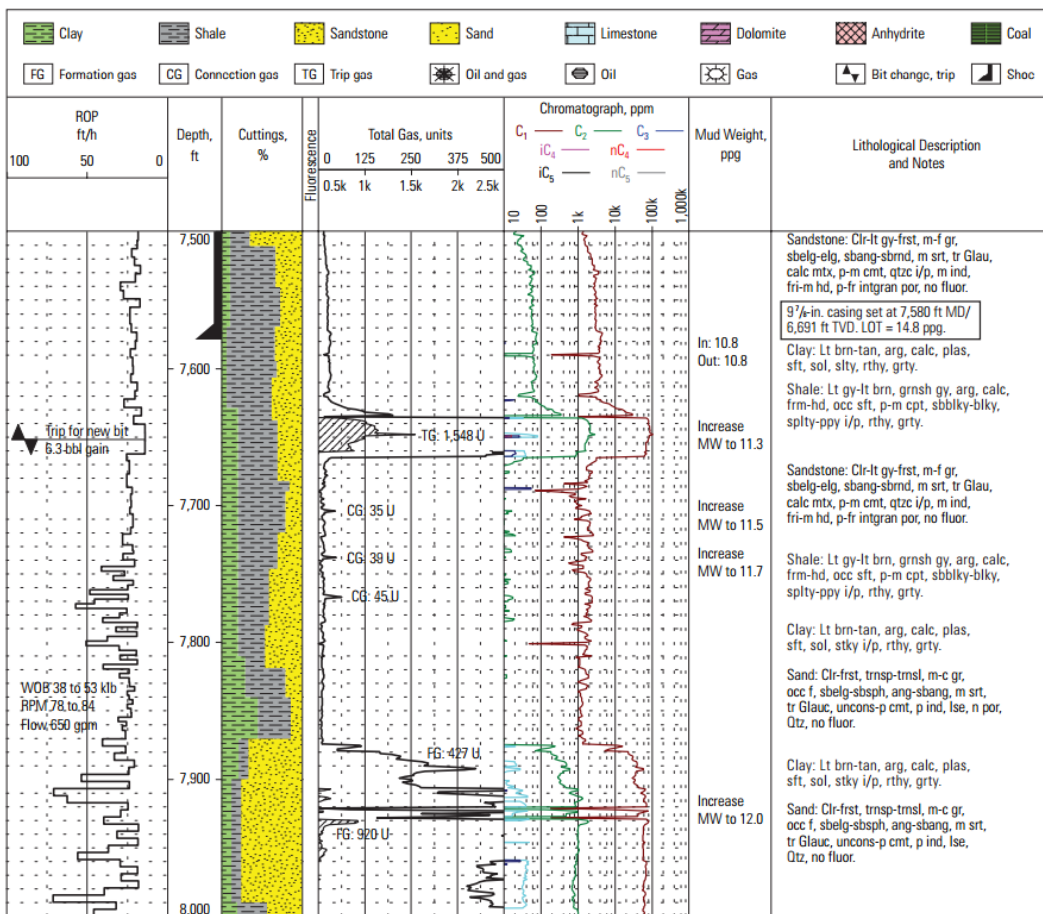
Figure 1-2: Mud logging report sample (Ablard, et al. 2012)

There has been a growing trend for drilling automation during the last decade. One of the focuses is real-time data monitoring and performance optimization for safety improvement in the wake of catastrophic events in this industry. For instance, the Macondo

incident, in April 2010, cost lives of 11 workers and billions of dollars (Huffington Post Canada 2014). This tragedy could have been avoided if the real-time data monitoring was performed correctly or automated. With the fast development of surface and downhole sensors, huge data is available for analyzing the performance of drilling operations. This work will present a unique computer vision system to monitor cuttings and cavings off the shale shaker system in real-time. Such system can assist mud logger and drilling operator to analyze downhole condition in real-time to improve work safety and drilling efficiency. Challenges remain in measuring accuracy in complicated operating environment and ease of system implementation. Multiple oil field visits were performed in order to identify an ideal approach to measure cuttings properties. Figure 1-3 illustrates the cuttings return system on a regular land rig. In this research study, the objective of the proposed design is to quantify volume, analyze size distribution, and regenerate surface profiles of moving cuttings in real-time.
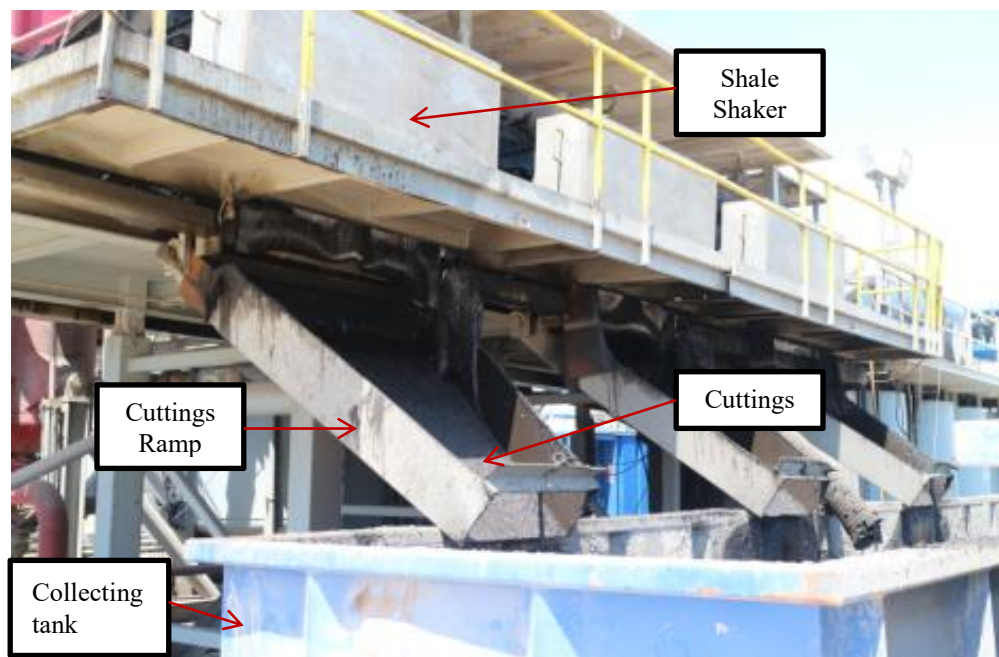
Figure 1-3: Cuttings return system on a land oil rig

1.2 CHAPTER DESCRIPTIONS

This thesis presents a computer vision application for real-time monitoring of cuttings in the oil and gas industry. An overview of the contents is listed below:

Chapter 2 reviews current techniques and approaches to measure cuttings and cavings properties at the oil rig. The advantages and limitations of each method are compared and evaluated. An understanding of the methodologies of these systems lays the foundation for the design of a new approach.

Chapter 3 gives a brief summary of cuttings and cavings properties and reviews current 3D sensing techniques. A clear understanding of all cavings shapes helps to select applicable computer vision techniques and sensors.

Chapter 4 reviews some empirical cuttings transport models for vertical and deviated wells. To expand the scope of this work one step further, this measurement should be linked to near real-time predictive models to form an automated monitoring system to improve the safety and efficiency of the drilling process.

Chapter 5 first presents how various sensors are evaluated and tested to meet the desired measurement resolution criteria. The computer vision algorithms are explained in detail. Lastly, an experiment setup is introduced to verify the capability of the proposed system.

Chapter 6 lists the experimental results and , analyzes these results to determine the viability of the proposed solution.

Chapter 7 gives a conclusion of this study and proposes some key objectives for the future work.

Chapter 2: Related Work

This chapter summarizes current techniques and methods which have already been applied to monitor cuttings/cavings properties in the industry. In addition, a review of existing conceptual designs and patents is also included to evaluate their advantages and disadvantages. The following review contains three sections: 1) existing intrusive systems for cuttings monitoring, 2) existing machine vision systems for cuttings monitoring, and 3) existing patents for cuttings monitoring.

2.1 EXISTING INTRUSIVE SYSTEM FOR CUTTINGS MONITORING

Monitoring cuttings/cavings properties brings valuable information on drilling process efficiency. This section provides an overview of some traditional and automated intrusive procedures which have been used/designed in order to "real-time" inspect cuttings/cavings properties.

2.1.1 Traditional Cuttings Size Measurement

One of the duties of a mud logger is to manually collect and examine some cuttings at different time intervals. The most common and old-fashion method is to obtain cuttings from flowline or "possum belly" as shown in Figure 2-1. The "possum belly" refers to the top part of the shale shaker where it holds the fluid mixture before it passes through shale shaker screen. Sometimes cuttings are also collected at the end of the shaker screen. One should keep in mind that shaker screen may lose some small particles depending on the shaker screen mesh size. (Karimi 2013)

Figure 2-1: Possum belly (Karimi 2013)

After wet cuttings are collected, a mud logger usually uses a series of sieves to sort out different size of cuttings and exposes the sieves to sunlight for drying the cuttings samples. The benefit of this simple sieve system is that it is easy to operate and costs little beyond the labor costs. An average mud logger annual salary is $64,000 in Texas (Indeed 2016). A mud logger can also easily differentiate cuttings and cavings on the sieve. As shown in Figure 2-2, a larger chunk caving was discovered on the sieve. However, this system requires continuous human intervention/labor. The accuracy highly depends on how frequently the mud logger performs the measurement and how representative the collected sample is. If a high percentage of clay is present in the drilling fluid, it increases the viscosity of the drilling fluid. As a result, clay/mud and cuttings tend to stick together in lumps as shown in the middle of Figure 2-2. Then it is impossible to collect and filter out a representative cuttings sample and perform accurate measurement. In addition, a mud logger regularly measures return mud weight to check if the shale shaker screen is filtering out fine particles efficiently. The biggest shortcoming is that this old-fashion procedure is not able to provide a reliable real-time measurement on monitoring cuttings/cavings volume, sizes, and shape.

Figure 2-2: Representation of sieve system (Karimi 2013)

2.1.2 Schlumberger CLEAR Cuttings Weighing System

The Schlumberger CLEAR service is a real-time cuttings weighing and monitoring system. It includes a cuttings flowmeter (CFM) and a weighing tray. The device is placed at the end of each shale shaker as shown in Figure 2-3. This product can be regarded as a large weighing scale. After the cutting pass by the shale shaker screen, they accumulate on the collecting tray at fixed time interval. The weight of the cuttings is then measured by strain gauges.   A mud-effect correction factor called the Equivalent Dry Cuttings Ratio (EDCR) is also applied to correct the errors caused by the coating of mud over the cuttings. At the end, the volume of equivalent dry cuttings is calculated. This real-time system also collects drilling parameters to calculate theoretical cuttings volume. By comparing the measured cuttings volume and theoretical return volume, the percentage of cuttings recovery can be used as a factor to reflect hole cleaning efficiency.

Figure 2-3: Schlumberger CLEAR hole cleaning and wellbore risk reduction service (Schlumberger 2015)

This real-time monitoring system is a commercial product by Schlumberger Company. According to Schlumberger case studies, the system is proven to improve drilling performance and minimize risk. However, questions remain on the volume calculation based on EDCR value. Drilling fluid not only coats the surface of the cuttings, but also invades into the cuttings. The amount of fluid invasion in the cuttings depends on mud rheology, lithology of the cuttings, and interaction time. Various factors may affect the EDCR accuracy. In addition, this system is not capable of detecting cavings, analyzing size distribution, and identifying shapes.

2.1.3 Cuttings Morphology

An automated cuttings sampling device was proposed by Arild Saasen, Tor H. Omland, Sigbjorn Ekrene et al in 2009 as shown in Figure 2-4. The system is placed in front of the shale shaker. An automated cup is applied to collect a small sample of cuttings. Then, the sample is transferred to section (3) for washing and drying. As described in the paper, section (5) is a particle analyzer, which is similar to a liquid particle analyzer. It uses a full frame photo-optical camera imaging system to determine the size distribution of the sample. After that, the sample is transferred to Raman spectroscopy, as section (7). The function of Raman spectroscopy is to detect the mineralogy of the cuttings (Jacqueline 2009).
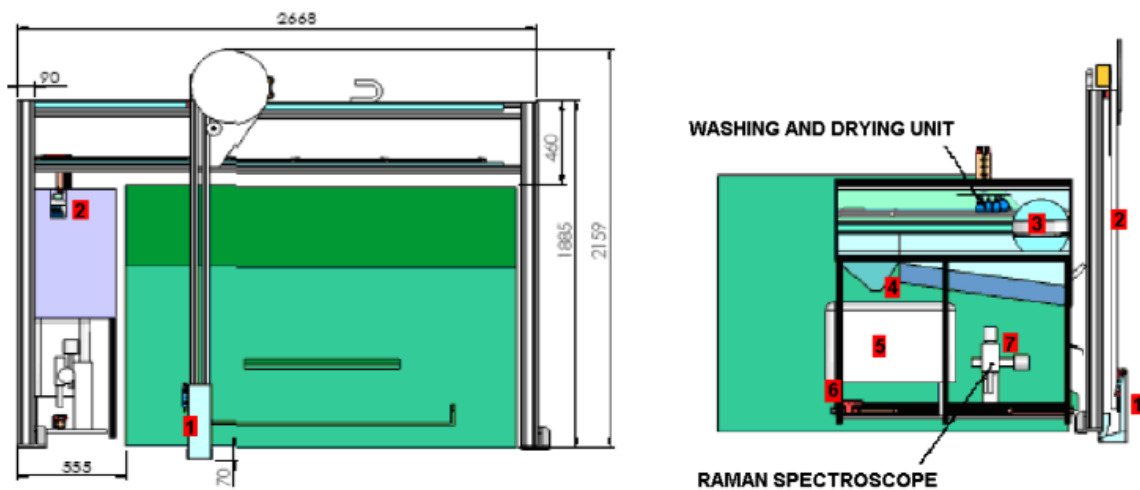
Figure 2-4: Schematic illustration of the cuttings morphology measurement device including position of the Raman spectroscope (Jacqueline 2009)

The advantages of this proposed design are cuttings cleaning, real-time measurement size distribution analysis, and mineralogy detection. However, no details about sensors and testing results were found in this publication. After searching through various sources, there is no sign that this proposed design has been commercialized.

Measurements of cuttings/cavings shape, dimensions, and length to thickness ratio of cuttings are mentioned but not detailed in this paper.

2.2 EXISTING MACHINE VISION SYSTEM FOR CUTTINGS MONITORING

This section describes two studies which have applied non-intrusive two-dimensional image processing techniques on monitoring cuttings/cavings.

2.2.1 Cavings Monitoring System

T.H. Omland from Statoil ASA has proposed a computer vision solution to measure the length to thickness ratio (L/T-ratio) of cavings (Omland, et al. 2007). It is possible to identify wellbore instability problems by analyzing the shape of cuttings and cavings. A field trial was performed as shown in Figure 2-5. In some cases, cuttings were treated with a small amount of fresh fluid in order to separate them from sticking together. Then imaging analysis was performed to determine sizes of cuttings/cavings and L/T-ratio.

Figure 2-5: Analysis of cuttings morphology. A trail of cuttings sample (left) and cuttings under 2D camera (right)(Omland, et al. 2007).

The author indicated that if the cutting had a uniform L/T-ratio, it meant no wellbore stability problems. The high aspect L/T-ratio indicates there were large cavings due to hole instability issue. Results from field study are presented in Figure 2-6. As the cuttings size became larger, the results showed no significant increase in the aspect ratio. This information was analyzed to indicate that no larger cavings existed. This research proposes a useful solution to measure cuttings size distribution and to analyze the shape of cavings by using L/T-ratio. Such measurements can reflect wellbore stability conditions in real-time. However, human intervention was still required to collect and prepare cuttings/cavings sample for further imaging analysis. In addition, the volume of return cuttings cannot be monitored.
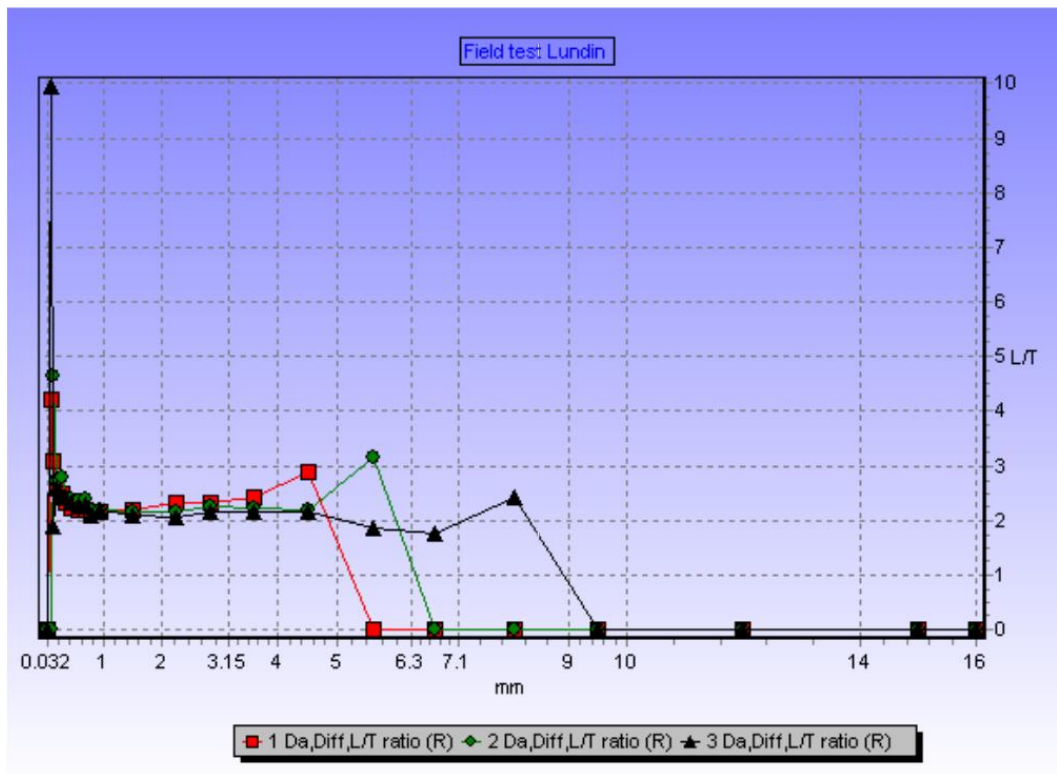
Figure 2-5: Aspect ratio of drilling cuttings (Omland, et al. 2007)

12

2.2.2 An Intelligent Drilling Cuttings Monitoring System

A non-intrusive computer vision system for real-time monitoring and analyzing of cuttings concentration at shale shaker was presented by A.N. Marana et al in 2010. The system used image processing techniques to directly monitor cuttings on a shale shaker screen. The gathered information helped indicate landslide and borehole wall collapse during drilling operations. As illustrated in Figure 2-6, a high definition camera was installed above shale shake and captured images were sent to a computer for further analysis. The system consisted of two modules: image acquisition and data analysis. During the drilling process, images of cuttings on shale shaker are classified to predefined classes. The analysis focuses on quantifying the concentration of cuttings on the surface based on data analysis module. This non-invasive measurement requires no field worker to operate. The algorithm analyzes each frame automatically and alerts a field operator if an abnormal pattern is spotted,
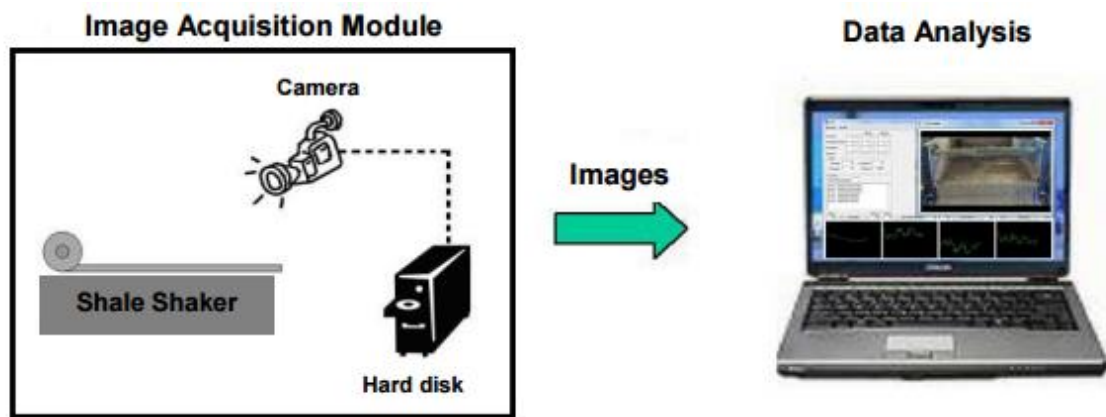
Figure 2-6: An intelligent drilling cuttings monitoring system architecture (Marana, et al. 2010)

The challenge of this technique is to capture an image of vibrating cuttings on a shale shaker screen. Intense image processing methods were applied together with modern artificial intelligence techniques, such as Optimum-Path Forest (OPF), Artificial Neural Network using Multiplayer Perceptrons (ANN-MLP), Support Vector Machines (SVM), and Bayesian Classifier (BC). An example of image analysis is shown in Figure 2-7. A field trial was conducted on an offshore drilling rig, and the system was demonstrated to monitor cuttings loading on shale shaker in real-time successfully. So far, this technique is the most automated non-intrusive computer vision system which has been validated in the field. However, the proposed system and algorithm cannot quantify cuttings volume, size, and shape. Cavings also cannot be differentiated from cuttings. The concentration of cuttings can only be used as a key performance indicator (KPI).
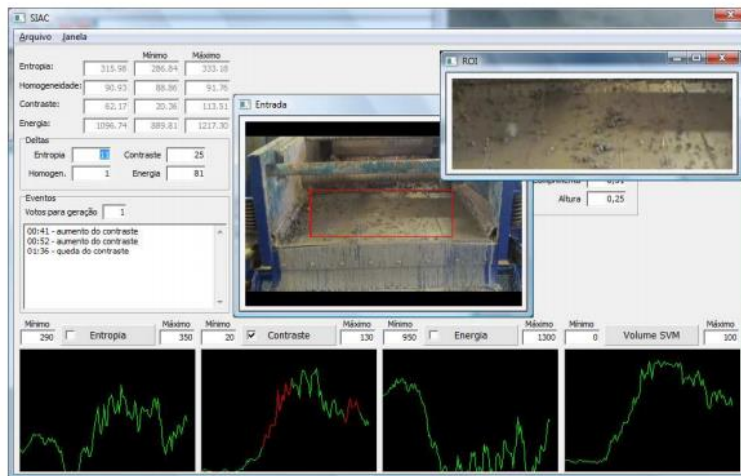
Fig. 2 – Actual version of the software.

Figure 2-7: Captured images are processed by the intelligent system (Marana, et al. 2010)

14

2.3 EXISTING PATENTS FOR CUTTINGS MONITORING

2.3.1 Down Hole Cuttings Analysis

This patent filed by Halliburton Company in 2013 describes a down hole cuttings analysis system, which applies surface computer vision system to monitor the characteristic features of return cuttings.   Such information can be analyzed to increase the effectiveness of pumping, sweeping, and drilling operations in oil and gas exploration. A schematic diagram is shown in Figure 2-8. A few key components of the patent are listed below (GRAVES and ROWE, Down hole cuttings analysis 2013):

- The system employs imaging device/apparatus to acquire image/video of cuttings. With potential illumination, one or more CCD (charge coupled device) cameras are included.

- Possible 3D facial recognition algorithm can be applied

- Cuttings size distribution, volume, and shape are analyzed in real-time

- A possible programmable data acquisition and memory system is used. Video can be streamed to remote workstation (Halliburton INSITE Anywhere web delivery system)

- Polarizers, filters and/or beam splitters (energy modifications devices) can be used to make drilling fluid become relatively transparent

- Analyzed data can be synchronized with other drilling operations parameters.
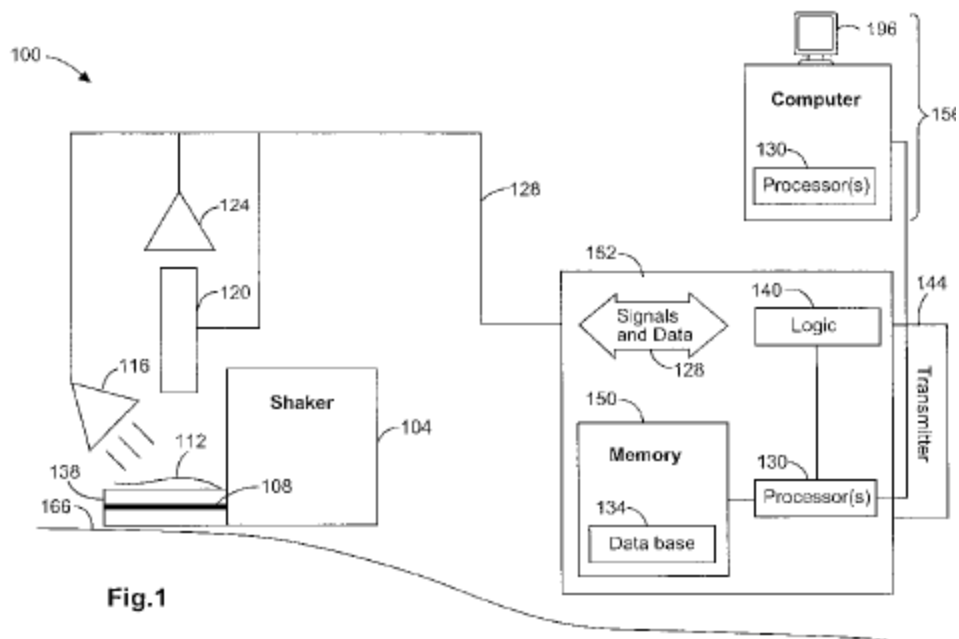
Figure 2-8: Patented concept for surface cuttings monitoring and analysis (GRAVES and ROWE, Down hole cuttings analysis 2013)

This patent detailed a potential fully automated computer vision system concept for real-time cuttings monitoring. Even though, no detailed 2D/3D vision techniques are described in the patent and no cuttings transport model is mentioned, this patent provides a good foundation to explore possible computer vision applications for cuttings/cavings monitoring.

2.3.2 System and Method for Improved Cuttings Measurements

This patent was also filed by Halliburton Company in 2012. The proposed systems and methods describe how to improve cuttings measurements by real-time continuous measurements of cuttings coming over shale shakers to predict the expected amount of cuttings. If the measured amount differs from predicted estimation, a warning alarm is sent.

The invention involves using a rotating helical screw (2) to measure cuttings from shale shaker (1) as shown in Figure 2-9. A motor (6) is set at a constant speed by a controller to rotate the helical screw (3). As the helical screw continually moves the discharged cuttings along the axis, weight sensors (4) measure the weight of cuttings in the device at a constant continuous manner. A baseline torque indicates the discharged cuttings are free of drilling fluid. By comparing the difference between actual torque and baseline torque, the percentage of fluid in the discharged cuttings is calculated. Then the total weight of dry cuttings can be estimated. Lastly, historical formation density is applied to calculate the volume of cuttings. Alarms can be activated to alert operators if the difference is not within a pre-established acceptable threshold. This proposed system is able to real-time quantify return cuttings volume, yet it cannot analyze cuttings/cavings size and shape.
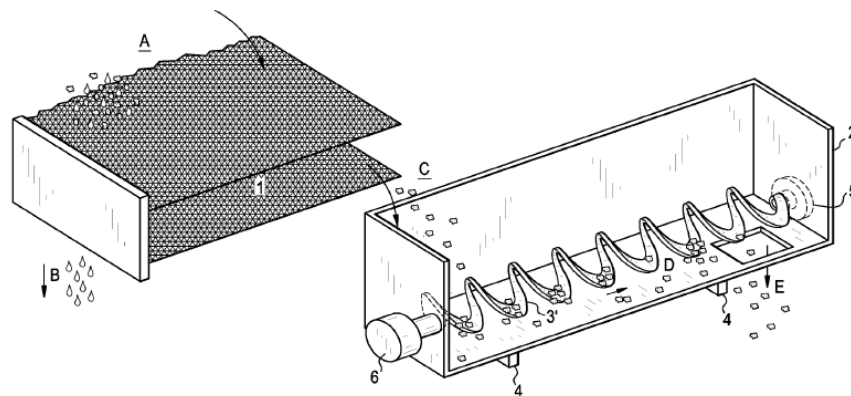
Figure 2-9: Patent concept for helical screw cuttings weighing system (SMITH 2012)

Summary of Existing Monitoring Systems

Previous sections present various techniques on measuring cuttings properties. Although a majority of these procedures and designs are detailed and some were tested, many of the systems or approaches have not been able to perform comprehensive

measurements or have not been prototyped. None of these systems can monitor cuttings volume, size distribution and cavings shape in real-time. Therefore, there still exists a need for solution to automate this cuttings monitoring process to improve drilling efficiency and safety.

2.4 EXISTING TECHNIQUES FOR ROCK MEASUREMENT IN MINING INDUSTRY

Bulk materials volume measurement is widely applied in mining industries. Initially, the bulk volume of mining materials based on the weight by a scale on a conveyor belt or a container and a fixed-value density factor. However, in many cases, measured material density is not homogeneous or constant and density is strongly influenced by humidity and rainfall. Then the volume calculation based on weight measurement becomes inaccurate. With the fast development in 3D scanning in the last decade, laser scanning analysis is now extensively adopted in mining industry to computing the volume value of bulk material on a conveyor belt system.

By positioning a laser scanner directly to moving rocks on a conveyor belt, the volume of the material is calculated at high speed and accuracy. The 3D depth of the rock surface is scanned at a high frequency and volume is calculated based on conveyor belt moving speed as shown in Figure 2-10. This kind of technique has also been applied in many areas like: open pit and underground mining, steel industry, food and beverages industry, bulk cargo transport and loading, etc. There are several commercialized available 3D scanners in the market like: Riegl LMS-20 (RIGEL 2010), Bulkscan LMS511 (SICK 2015), LaseBVC (LASE 2013), and Walz Load Scanner (Walz 2014).
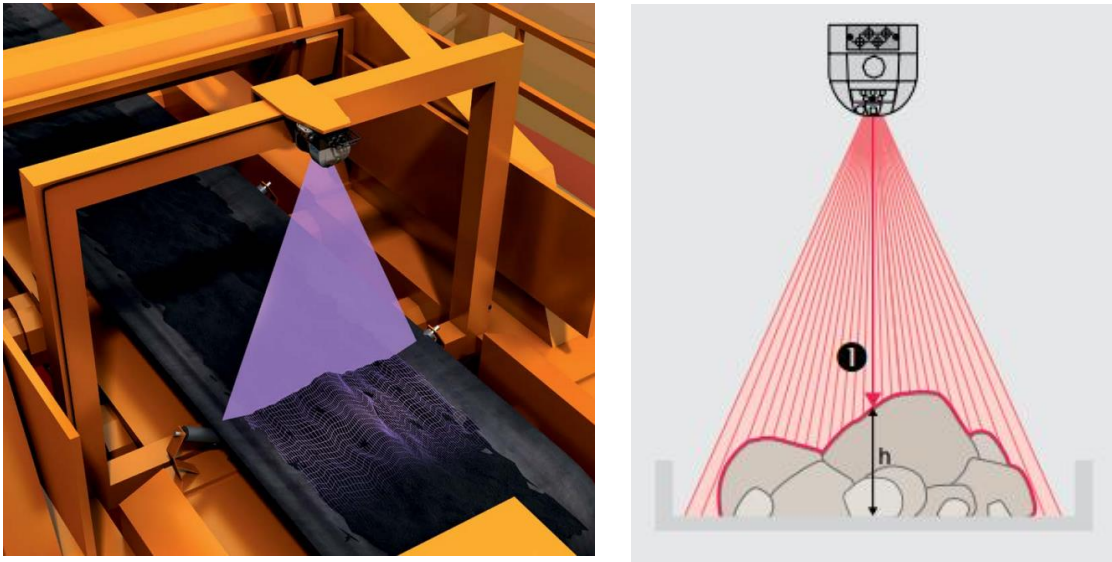
Figure 2-10: A laser sensor scanning the volume of bulk material on a conveyor belt (left) and scanning mechanism (right) (SICK 2015)

The advantages of this laser technique are non-intrusive measurement, fast scan rate, accurate volume calculation, 3D profile modeling, low maintenance, and robustness. This application of 3D scanning techniques provides a potential solution to measure the volume of a moving target. However, these applications have a resolution of 0.5 to 1 meters (LASE 2013). Higher resolution scanners are required in order to measure drilling cuttings. In addition, a conveyor belt system does not exist on most land oil rigs. Therefore, if a similar 3D scanning technique is applied, an accurate speed tracking system should be designed to serve the function of an encoder on a conveyor belt.

Chapter 3: Literature Review

The previous chapter provided a detailed overview of current applications for measuring cuttings/cavings properties. The advantages and disadvantages of each system are discussed based on their measuring accuracy, functionalities, and feasibility. The primary objective of a cuttings monitoring system is to real-time quantify cuttings volume and to build a three-dimensional profile of cuttings and cavings. The following sections are intended to review the properties of cuttings /cavings and to summarize standard methods that a computer vision system can use to perform the three-dimensional measurement. An understanding of 3D sensing algorithms provides a solid base for designing a computer vision system for real-time cuttings monitoring. Extensive review of the literature related to modeling the returned cuttings was also completed, but is presented separately in Chapter 4.

3.1 A REVIEW ON DRILLING CUTTINGS AND CAVINGS

In the oil and gas industry, drilling cuttings are defined as rock debris which are transported to the surface by the drilling fluid. Small pieces of rock are dislodged due to the interaction with a drill bit. After being transported from a wellbore to the surface, cuttings are treated by shale shaker system to screen out the drilling mud. A mud logger engineer commonly examines the subsurface formation properties through collected drilling cuttings. Information such as, composition, size, shape, color, texture, and hydrocarbon content are recorded and documented. Cuttings size and shape are usually determined by drill bit type and cutting mechanism. The figure below shows how formation interacts with different types of drill bits.
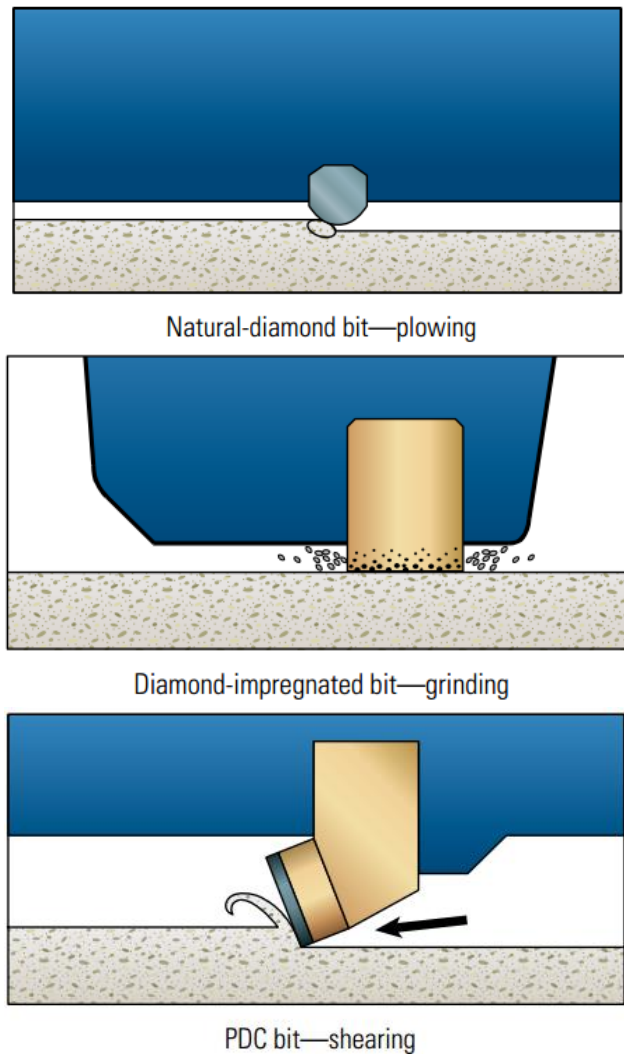
Figure 3-1: Different cutting mechanisms of drill bit (Bruce Burr 2000)

Compared with regular drilling cuttings, caving fragments are different and visually noticeable in size and shape. Cavings are normally two to three times larger and have odd shapes (D. Kumar 2012). In most cases, cuttings larger than half an inch are considered as cavings. The following figure briefly summarizes how different types of cavings are formed.

Caving Type	Shape	Description	Cause	Solution
Tabular		Flat and parallel surfaces	Rubble zones, brittle rock	Adjust mud weight, change mud type, reduce surge and swab
Angular		Non-parallel angular edges, rough surface structure	Borehole break-out, shear failure	Increase mud weight and flow rate
Splintered		Long, concave shape	Enlarged wellbore, tensile failure, stress in massive shales	Increase mud weight, change trajectory

Figure 3-2: A summary of cavings types (Karimi 2013)

The shapes of cavings can be categorized as tabular, angular, and splintered. The shapes of cavings indicate different mechanisms which cause wellbore collapsing. The size of cavings can be measured based on length, width, and thickness. Cavings provide an indication of possible wellbore instability, formation overpressure, and overall well behavior. Cavings can be induced by underbalanced drilling, stress relief, pre-existing planes of weakness or mechanical action by drilling tools (D. Kumar 2012). Real-time monitoring of cavings during drilling operations can help optimize drilling performance by using appropriate actions to prevent non-productive time. This motivates the need for a real-time monitoring system to differentiate cavings from cuttings and to recognize cavings shape.

3.2 THREE-DIMENSIONAL VISION TECHNOLOGIES

Three-dimensional (3D) vision techniques measure the physical distance between a target surface and sensor's reference position. Various technologies can be applied for range measurement, 3D modeling, object detection, and many other sensing applications. In the past decade, 3D sensing technologies have been developing tremendously. This advanced technology is mostly applied for computer vision and automation applications. The following sections will review the methodologies of three major 3D sensing techniques: stereo vision, time-of-flight, and structured light.

3.2.1 Stereo Vision

Stereo vision is one of the most popular 3D sensing techniques and was developed before other 3D technologies. This technique aims to extract 3D depth information from digital images. Two charge-coupled device (CCD) cameras are commonly used to capture images. The CCD sensor is a silicon based multichannel array etched on an integrated circuit for detecting UV, visible, and near-infra light (Edwards 2001). Traditionally, two identical CCD cameras are placed horizontally at a fixed distance as shown in Figure 3-3. By analyzing the differences in the two images, the relative depth can be calculated. This is similar to human binocular vision. To calculate the depth value Z of target P, U_L and U_R represents the x-coordinates of P projection on two image planes, where $U_L = f\frac{X}{Z}$ and $U_R = f\frac{X-b}{Z}$. f is the focal length of the camera. Then a disparity value d is calculated as $d = U_L - U_R = f\frac{b}{Z}$. At last, the actual distance between target P and the stereo sensor can be calculated as $Z = f\frac{b}{d}$. (National Instruments 2012)
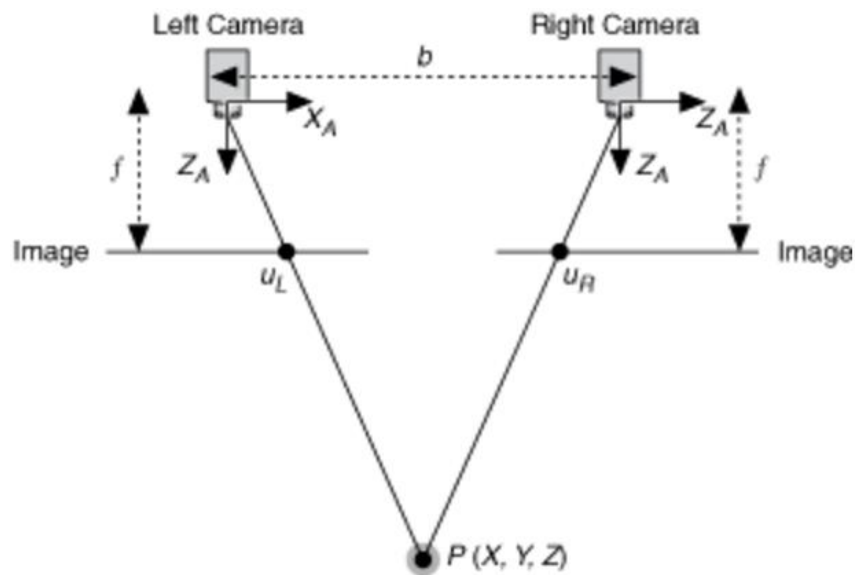
Figure 3-3: Principle of operation for stereo vision (National Instruments 2012)

The depth resolution of the sensor relies on camera's focal length, image resolution, and baseline. On the other hand, stereo vision requires long computation time in order to apply multiple feature detection to compare two images. Therefore, it is more suitable to 3D scan static objects or scan at low frequency. Because of its simplicity and low cost, 3D stereo vision system is widely used in robotics and other automated systems for machine vision application. One of the most common stereo vision cameras is Point Grey Bumblebee2 as shown in Figure3-4. Military grade systems like MultiSense S21 and SL (Carnegie Robotics 2016) are also designed and manufactured by Carnegie Robotics for robotic applications in rough outdoor environment.

Figure 3-4: Point Grey Bumblebee2 Stereo Vision Sensor (Point Grey 2016)

3.2.2 Time-of-Flight

A 3D time-of-flight (ToF) camera measures the distance to a target by emitting a modulated light to the target and observing the reflected light. The basic concept is illustrated by Figure 3-5. Two methods can be used to calculate the object's distance. One method is measuring the reflection time and calculating the distance based on the speed of light. The other method is to translate phase shift between the emitted signal and received signal to a distance value. Most illumination source used is a solid-state laser or a light-

emitting diode (LED). The wavelength of the light is about 850 nm (near-infrared visible light) (Li 2014).   In order to detect the phase shift between the emitted signal and received signal, either pulsed or continuous-wave modulated signal can be used.
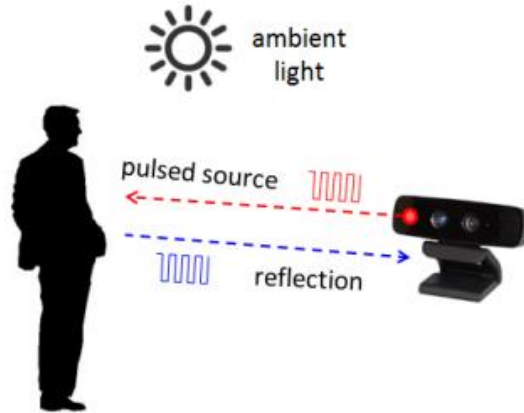
Figure 3-5: 3D time-of-flight camera operation (Li 2014)

The advantages of ToF 3D vision system are fast computational speed, high resolution, and low cost. One concern is that if the emitted light wavelength is in the range of background light, the detection might be suppressed. This technology has been widely applied in human-machine interfaces and gaming. In some industrial machine vision, ToF cameras are also used for quality inspection and object detection. In the aviation industry, ToF sensor is installed on an areophane to obtain digital elevation models of the Earth's surface. There are a variety of commercial cameras such as the Creative SENZ3D as shown in Figure 3-6.

Figure 3-6: Creative SENZ3D ToF Camera (CREATIVE 2016)

3.2.3 Structured Light

The structured light vision system is a well-established technique for range measurement and 3D modeling. The principle of operation is to project a band of light onto the target's surface. A camera or multi cameras are used to observe the distorted light pattern on the illuminated surface (David Fofi 2004). The band of light has a predefined pattern as gray codes, light stripes, sine waves, or speckle patterns (Geng 2011). To explain the detecting algorithm, a single camera structured light system is used as an example shown in Figure 3-7. Projector emits a beam of patterned light on to an object. Each pixel of the projector has a specific local configuration of the projected pattern. By comparing with the distorted projection pattern on the target surface, the 3D geometric shape or profile of the target surface can be computed by various algorithms (Pietro Zanuttigh · Giulio Marin 2016).
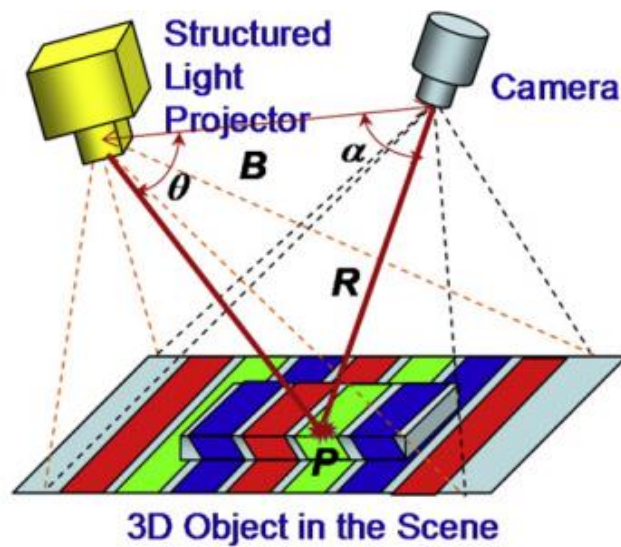
Figure 3-7: Illustration of structured light (Geng 2011)

There are two major methods to generate a strip pattern: laser interference and projection. The laser interference technique projects a single strip of laser light. The interference has regular and equidistant dots in the line pattern. Then the height of the target surface is calculated by triangulation method (Figure 3-8). This method generates a very precise 2D profile of the surface. The laser interference can scan at high frequency and is less affected by ambient lighting condition. The projection technique emits incoherent light with coded pattern (Figure 3-9). Instead of scanning one line each time, the method takes a "snap-shot" over a target's surface. This method has the advantage of fast 3D scanning. However, compared to the laser interference, the coded projection light is strongly suppressed by the ambient lighting environment.   In general, the structured light vision system is the most applied technique for volume measurement, 3D model reconstruction, surface regeneration, reverse engineering, optical inspection, and shape measurement.
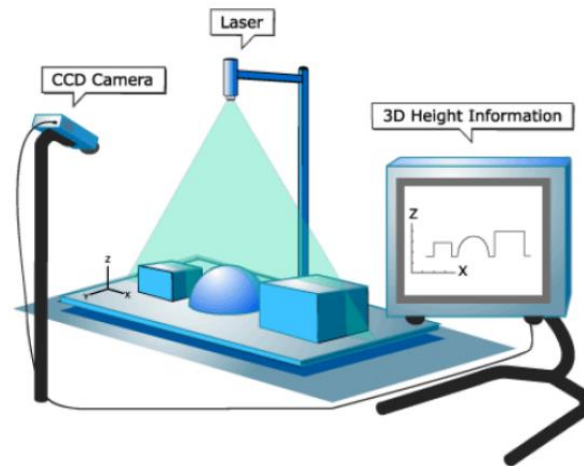
Figure 3-8: Laser scan based on triangulation (Gerig 2013)
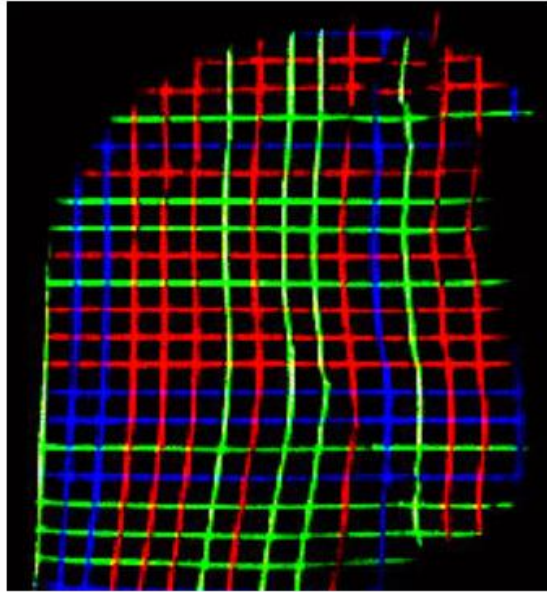
Figure 3-9: An example of color-coded grids (Geng 2011)

Summary of 3D Vision Techniques

The section above provided an overview of current 3D sensing techniques which can be applied for real-time cuttings monitoring. It is important to understand the working mechanism of each technology in order to select a suitable vision system to meet the desired accuracy. The following table summarizes the advantages and disadvantages of each system with regards to: depth accuracy, scanning speed, distance range, low light performance, outdoor performance, software complexity, and cost. In Chapter 5, selected vision system are tested and evaluated.

Table 3-1: 3D vision system comparisons (Michael Brading 2016)

	Stereoscopic Vision	Structured Light		Time of Flight
		Fixed Pattern	Programmable Pattern	
Depth Accuracy	mm to cm *Difficulty with smooth surface*	mm to cm	µm to mm *Variable patterns & different light sources improves accuracy*	mm to cm *Depends on resolution of sensor*
Scanning Speed	Medium *Limited by software complexity*	Fast *Limited by camera speed*	Fast/Medium *Limited by camera speed*	Fast *Limited by sensor speed*
Distance Range	Mid range	Very short to mid range *Depends on illumination power*	Very short to mid range *Depends on illumination power*	Short to long range *Depends on laser power & modulation*
Low Light Performance	Weak	Good	Good	Good
Outdoor Performance	Good	Weak/Fair *Depends on illumination power*	Weak/Fair *Depends on illumination power*	Fair *Depends on illumination power*
Software Complexity	High	Low/Middle	Middle/High	Low
Material Cost	Low	Middle	Middle/High	Middle

Chapter 4: Cuttings Transport Models Review

The primary objective of this project is to design a computer vision system for quantifying cuttings return volume in real-time. The measured cuttings volume also serves as an important indicator for hole cleaning efficiency. An accumulation of excessive drilling cuttings in the annular space can lead to mechanical drill pipe stuck by either creating more differential sticking or blocking bottom hole assembly. To expand the work one step further, it is essential to incorporate a cuttings transport model for estimating the theoretical cuttings return volume based on drilling parameters. Such a system can continuously compare the difference between the measured volume and the theoretical return volume of cuttings in real-time. In addition, cuttings size distribution and cavings also represent borehole quality and formation strength. With the assist of a comprehensive cuttings transport model, the traveling time of cuttings and cavings can be estimated. A field operator can then relate the measured cuttings characteristics and cavings to the depth where this debris was produced. This chapter provides a brief overview of some well-established cuttings transport models. An awareness and understanding of the models provide a solid foundation to designing a sophisticated cuttings/cavings real-time monitoring system.

4.1 CUTTINGS TRANSPORT BEHAVIOR IN WELLBORE

In drilling operations, cuttings are transported to the surface by drilling mud through annular space. Due to gravity effect, rock debris tends to settle in the moving fluid. The situation is more complicated by the velocity distribution of moving fluid in the annulus and hole inclination angle. The following schematic represents cuttings transport mechanisms in vertical and deviated wells.
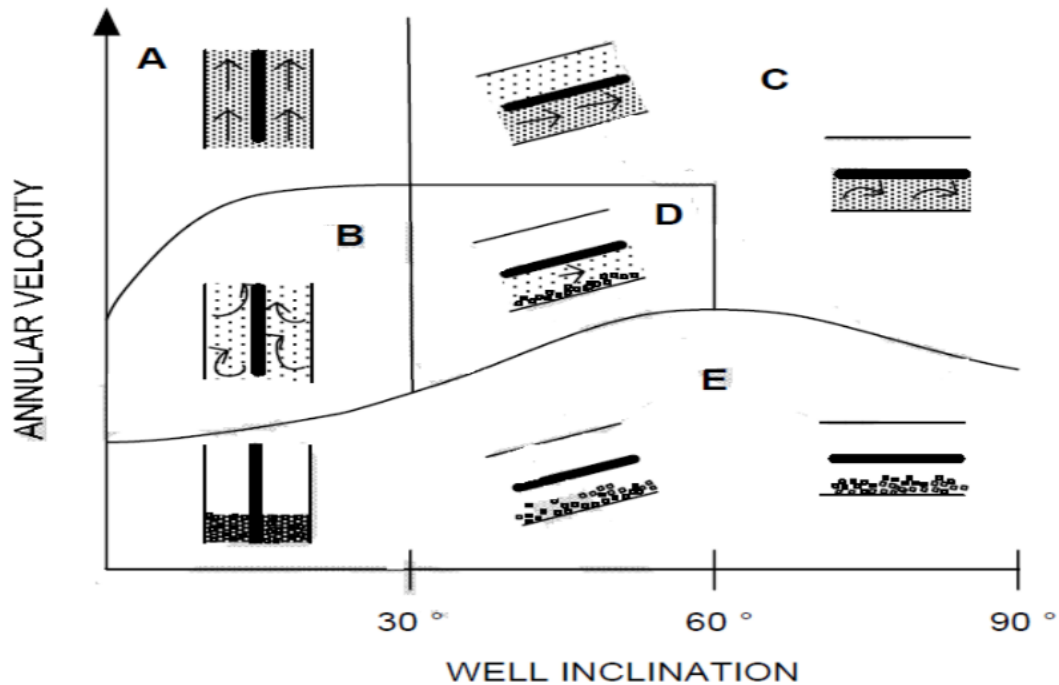
Figure 4-1: Cuttings transport mechanisms in vertical and deviated wells (API 2009)

Figure 4-1 illustrates different scenarios of cuttings transport behavior based on well inclination angle and annular fluid velocity. In the annulus, cuttings traveling velocity can be affected by various factors: mud flow rate, cutting/particle size, drill pipe eccentricity, drill pipe rotation, hole size and hole angle, drilling fluid rheology, rate of penetration, multi-phase flow effect, and effect of cutting bed accumulation (Tobenna 2010). All these factors complicate the process of estimating the cuttings settling velocity. Due to these difficulties, most cuttings transport model are empirical, based on experimental studies of drilling fluid carrying capacity.

31

4.2 SUMMARY OF CUTTINGS TRANSPORT MODELS

In order to estimate the cuttings traveling velocity, it is necessary to know the slip velocity (v_s) of the particle. The slip velocity is defined as the rate at which a particle falls in stagnant fluid. Then cuttings traveling velocity for vertical well can be calculated as:

$$v_{traveling} = v_f - v_s$$

Where, v_f is the fluid velocity in the annulus.

The following two tables summarize some of the popular models to estimate cuttings slip velocity and traveling velocity. Note that for high angle deviated wells, the cuttings traveling velocity is a combination of cuttings slip velocity and minimum flow rate based on the hole angle. Table 4-1 summarizes cuttings slip velocity models for vertical well and Table 4-2 summarizes cuttings slip velocity models for highly deviated well.

Table 4-1 Summary of vertical cuttings transport models

Source	Cuttings Slip Velocity (v_s)
(Cranford 1992)	Cuttings size > 0.001m: $$v_s = 1.1 \sqrt{(\frac{\rho_p}{\rho_f} - 1)gd}$$
(Chien 1971)	For irregular particles in non-Newtonian fluids: $$v_s = 0.45 \left(\frac{\mu_f}{d\rho_f}\right) \left[\left(\frac{36800}{(\frac{\mu_f}{d\rho_f})^2} d \left(\frac{\rho_p}{\rho_f} - 1\right) + 1\right) - 1\right]^2$$ For normal drilling fluid and cuttings sizes: $$v_s = 86.5 \sqrt{d(\frac{\rho_p}{\rho_f} - 1)}$$

Table 4-1 Summary of vertical cuttings transport models

(Chien, 1994)	For frequently occurring irregular particles in a turbulent-slip regime: $$v_s = 120.0 \left(\frac{\mu_e}{d\rho_f}\right)\left[\sqrt{1 + 0.0727 \left(\frac{\rho_p}{\rho_f} - 1\right)\left(\frac{d\rho_f}{\mu_e}\right)^2} - 1\right]$$
(Moore 1974)	In power-law and Newtonian fluids: Reynolds's number > 300: $$v_s = 1.54 \sqrt{d(\frac{\rho_p - \rho_f}{\rho_f})d}$$ 3 < Reynolds's number < 300: $$v_s = \frac{290d(\rho_p - \rho_f)^2}{\rho_f^{0.333}\mu_e^{0.667}}$$ Reynolds's number < 3 : $$v_s = 82.87 \frac{d^2}{\mu_e}(\rho_p - \rho_f)$$
(Zeidler 1972)	In power-law and Newtonian fluids: 2 < Reynolds's number < 15: $$v_s = 13.42 \frac{(\rho_p - \rho_f)^{0.782}}{\rho_f^{0.218}} \frac{d^{1.35}}{\mu^{0.564}}$$ 15 < Reynolds's number < 80: $$v_s = 13.88 \frac{(\rho_p - \rho_f)^{0.612}}{\rho_f^{0.388}} \frac{d^{0.836}}{\mu^{0.224}}$$ 80 < Reynolds's number < 1500: $$v_s = 17.88 \frac{(\rho_p - \rho_f)^{0.516}}{\rho_f^{0.48}} \frac{d^{0.548}}{\mu^{0.032}}$$

where μ_e = effective viscosity, d = particle nominal/equivalent diameter, ρ_f = drilling fluid density, and ρ_p = particle density.

Table 4-2 Summary of high angle cuttings transport models

Source	Cuttings Slip Velocity (v_s) and Traveling Velocity (v_{ct}).
(Larsen 1990)	For inclination angle $50° < \theta < 90°$: $$\overline{v_{eslip}} = 0.00516\mu_a + 3.006 \; if \; \mu_a < 53cp$$ $$\overline{v_{eslip}} = 0.00516(\mu_a - 53) + 3.28 \; if \; \mu_a > 53cp$$ General equivalent slip velocity: $$v_{es} = C_\theta C_d C_{mw} \overline{v_{eslip}}$$ The inclination angle correction factor: $$C_\theta = 0.0342\theta - 0.000233\theta^2 - 0.213$$ The cutting size correction factor: $$C_d = -1.04d + 1.286$$ The mud weight correction factor: $$C_{mw} = 1 - 2.779 \times 10^{-4}(\rho_f - 1042.5) \; if \; \rho_f > 1042.5 \; kg/m^3$$ $$C_{mw} = 1 \; elsewhere$$
(C.J. Hopkins 1995)	Vertical slip velocity: $$v_s = \frac{((\rho_p - \rho_f)^{0.667} \times 175 \times d)}{\rho_f^{0.333}\mu_a^{0.333}} \times FMW$$ FMW is correction term due to the effect of mud weight: $$FMW = 2.117 - 0.1648\rho_f + 0.003681\rho_f^2$$ The minimum cutting traveling velocity: $$v_{ct} = v_s cos\theta + v_2 sin\theta$$ Where: $$v_2 = C \times \left[\left(\frac{\rho_p - \rho_f}{\rho_f}\right) g^3 \left(\frac{d_h - d_p}{12}\right)^3\right]^{1/6}$$

Table 4-2 Summary of high angle cuttings transport models

(Rubiandini 1999)	Vertical slip velocity is based on Moore's model For inclination angle $\theta < 45°$ $$v_s = \left[1 + \frac{\theta(600 - RPM)(3 + \rho_f)}{202500}\right] v_{s\_Moore}$$ For inclination angle $\theta > 45°$ $$v_s = \left[\frac{(600 - RPM)(3 + \rho_f)}{3000}\right] v_{s\_Moore}$$

Where $\overline{v_{eslip}}$ = equivalent slip velocity, μ_a = apparent viscosity, d = particle nominal/equivalent diameter, ρ_f = drilling fluid density, ρ_p = particle density, d_h = hole diameter, and d_p = drill pipe diameter.

As an important element of the real-time cuttings monitoring system, a cuttings transport model is essential for predicting theoretical cuttings return volume and traveling time in order to make assessment when comparing to the measured value. While the experimental evaluation of these models is not within the scope of this effort, they do drive the requirements for the experimental system that will be designed and evaluated in Chapters 5 and 6. The key requirements derived from the future need to evaluate these models are:

- The system can real-time quantify cuttings volume at high accuracy.
- Computation time should be kept in minimum.
- Software design should be able to include field drilling parameters.
- In all of the models above, required drilling parameters are necessary to be acquired in field experiments in order to theoretically estimate cuttings return volume and traveling time.

Chapter 5: Sensors Selection, Methodology and Experiment

In Chapter 3, an overview of various available 3D depth sensing techniques that can be applied to measure cuttings/ cavings physical properties was presented. This chapter first provides a summary of selected sensors which were tested and evaluated in order to satisfy the desired accuracy of measuring drilling cuttings. The specifications of hardware and software of each sensor were examined to evaluate their advantages and disadvantages respectively. Secondly, a unique integrated computer vision design is proposed to function as a real-time measuring system to quantify the cuttings volume and size distribution. The algorithm is described and the software architecture is illustrated in sufficient detail to demonstrate the capability of the design. Finally, the experiments performed to validate the design concept and test the measuring methodology is described. Details of field testing and system model will be discussed in Chapter 6.

5.1 SENSORS SELECTION AND TESTING

Section 5.1 describes the selection of available 3D depth sensors and 2D HD cameras. It is crucial to test and analyze 3D sensors in order to achieve desired measurement and accuracy. In Chapter 3, three types of 3D sensing techniques have been presented. The following table compares five different depth sensors and some key technical parameters.

Table 5-1: Comparison of five 3D depth sensors

	Kinect 3D Sensor	ENSENSO N20	SICK LMS400-2000	Acuity 820 – 1000	Gocator-2380
Type	Structured Light	Structured Light	Laser	Laser	Laser
Scanning Frequency	30 fps	10, 30 fps	200-500 Hz	≤ 200 Hz	≤ 5000 Hz
Resolution	mm to cm	$\leq$8mm	$0.1° – 1.0°$	≤ 1mm	$\leq$1mm
Distance Range	Mid	Short	Mid to long	Mid to long	Mid to long
Outdoor Performance	Weak	Weak	Good	Good	Good
Cost	Low	High	Medium	High	High

5.1.1 3D Structured Light Sensor Testing

In the section, Microsoft Kinect sensor and ENSENSO N20 sensor are evaluated to analyze their feasibility to quantify drilling cuttings and cavings volume. Both cameras are structured light 3D sensors.

Kinect Sensor

Microsoft Kinect sensor was first launched to market in November 2010 and is an accessory to the Microsoft Xbox 360 video gaming console (Alex 2009). It is equipped with one IR emitter, one color sensor, one IR depth Sensor, and a tilt motor as shown in Figure 5-1. The IR emitter emits infrared laser beams with a projected speckle pattern and the depth of object is calculated based on reflected light. The RGB color camera has a resolution of 640 x 480 with a frame rate of 30 frames per second (fps). The 3D depth sensor has a resolution of 320 x 240 at 30 Hz (Zennaro 2014). The nominal depth range is from 0.8 m to 3.5 m. In the meanwhile, the nominal depth resolution is about 1 cm at 2 m distance (M.R. Andersen 2012). The depth sensitivity of the IR receiver strongly depends on the distance to the object and the ambient lighting environment. After Microsoft released their full Software Development Kit (SDK), Kinect sensor has been widely applied in robotic and computer vision research. The cost is relatively low (less than $150). The camera is powered by a 12V supply and has a custom cable (USB connection) for data transmission. In 2014, a newer generation Kinect V2 has also been released with high resolutions in depth sensing (Microsoft 2016).
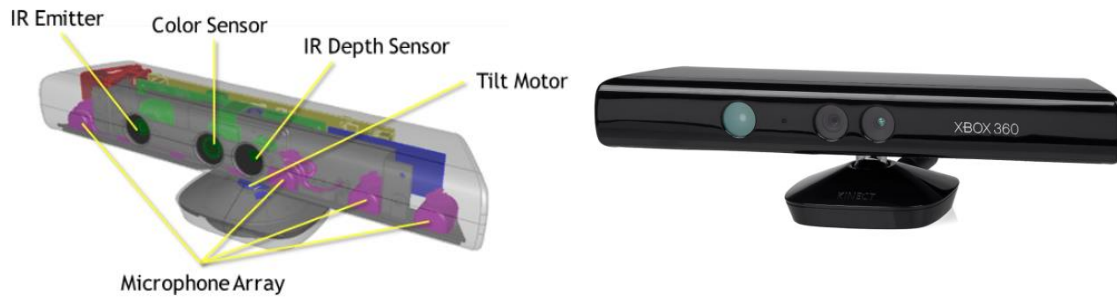
Figure 5-1:   Microsoft Kinect sensor for Xbox 360 (Microsoft, Kinect for Windows Sensor Components and Specifications 2010)

To test the feasibility of the Kinect sensor, the camera was mounted 1m from the ground pointing vertically to some rock samples. The sizes of the rocks were ranging from 10 mm to 60 mm. The testing was performed on static rock samples in indoor lighting environment. As shown in Figure 5-2, the left figure is an RGB color image and the right figure is a 3D depth image. Kinect depth sensor is capable of generating a 3D profile of rock samples. However, the accuracy dropped dramatically as the rocks started to move. In addition, rock samples less than 3 mm could not be captured by the depth sensor even at the optimal lighting environment. An outdoor testing was performed by Mauro Dalla Mura et al.(2012). The Kinect sensor was tested for granulometry to estimate the sizes of grains of gravel surfaces in an outdoor environment (Figure 5-3). According to the research results, even though the Kinect sensor served as a portable and low-cost 3D depth sensor, accuracy is affected by direct sun illumination. The sunlight causes saturation issues in depth acquisition. In addition, it has also been discovered that the heated surfaces might have an effect on receiving the reflected IR pattern which determines the 3D depth accuracy.

Therefore, the Kinect sensor is not suitable for the desired functionality in the oil field   for measuring cuttings/cavings volume and 3D depth profile in real-time. Not only

can the Kinect sensor not achieve high accuracy, but also its performance is strongly jeopardized by illumination environment, object's movement, and surface temperature.
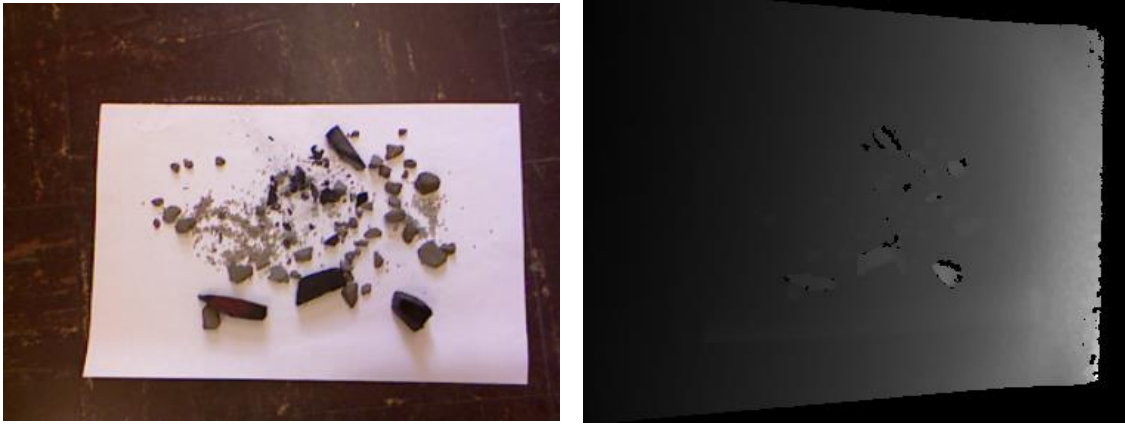
Figure 5-2:   RGB image (left) and 3D grayscale depth image (right) by Kinect sensor
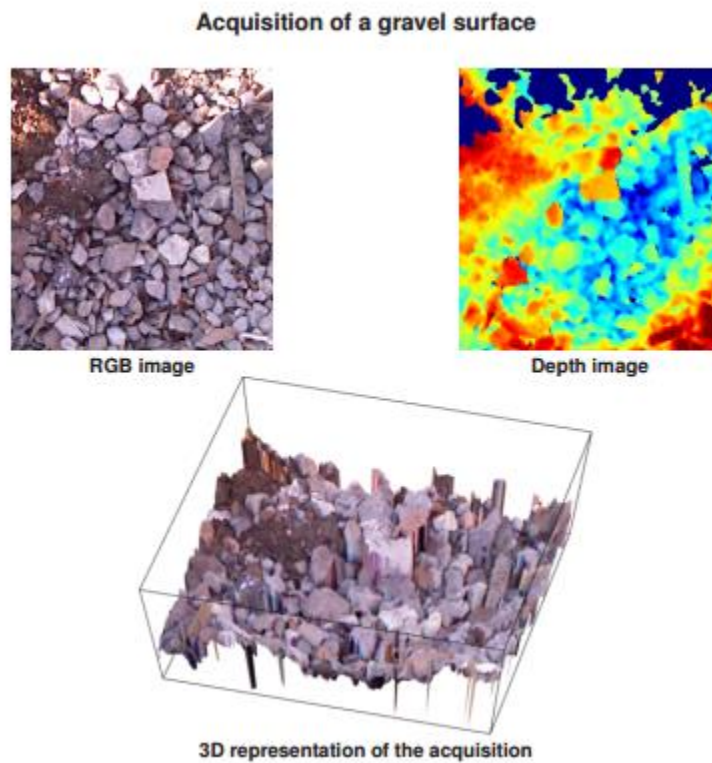
Figure 5-3:   3D acquisition of a gravel surface (Mauro Dalla Mura 2012)

Ensenso N20

Ensenso N20 stereo 3D camera also uses the principle of projected texture stereo vision. Ensenso stereo camera is a high-resolution camera which is widely equipped in manufacturing and quality inspection industry. The model has two integrated complementary metal-oxide-semiconductor (CMOS) sensors and a projector. The measuring object is cast with certain random point pattern from the projector. Compared to Kinect 3D sensor, Ensenso stereo 3D applies triangulation calculation by image comparison and projection of static, unknown pattern with the advantage of two CMOS cameras. The sensor has a scanning frequency of 30 fps with a resolution 1280 x 1024. It generates a much higher accuracy ranging from 0.03 mm to 8 mm at a distance of 0.2 m to 2 m. The robust and compact camera housing has a dimension of 175 mm x 50 mm x50 mm (IDS, Ensenso N20 Stereo 3D camera 2014). The power supply is via Power over Ethernet (PoE) with 12 – 24V. The advantage of PoE is that it can transmit data to a PC terminal up to 100 meters away at a high bandwidth. However, this industry standard 3D depth camera has a much higher cost compared to Kinect sensor. The retail price is above $15,000.
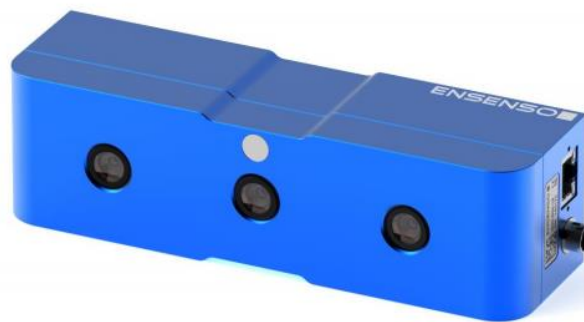
Figure 5-4:   Ensenso N20 Stereo 3D camera (IDS, Ensenso N20 Stereo 3D camera 2014)

Due to the availability of this product in the United States, a demo sensor was not available for testing. However, the manufacturer sent a few testing samples. As shown in Figure 5-5, it has been demonstrated that Ensenso camera can capture 3D profile of a moving object with rich details. On the other hand, similar to Kinect sensor, emitted structured light from Ensenso stereo camera is also limited to ambient lighting environment. The camera has to be placed close (at about 0.8m) to subject in order to achieve high depth resolution. Even so, the field of view is reduced and this makes it difficult to measure an object with large surface area.

Figure 5-5:   (Left to right) a) Sensor mounted on a moving robotic arm b) RGB image c) 3D point cloud profile of objects (IDS, Obtaining Depth Information from Stereo Images - Whitepaper 2012)

To summarize 3D structured light sensors, both of these three-dimensional vision systems can be applied to quantify the volume of measuring subject and to generate a detailed 3D depth profile. In the meanwhile, Kinect sensor is limited to its accuracy and robustness. Ensenso 3D cannot achieve the desired accuracy without sacrificing FOV. Multiple Ensenso cameras might be required in order to be employed in this application, which will not be cost effective. As a result, current 3D structured light sensors are not recommended for measuring cuttings/cavings volume and depth profile. However,

technology is developing fast in stereo vision system and there might be a more suitable 3D structured light camera for the oil and gas industry in the near future

5.1.2 Laser Profile Scanner Testing

Laser profile scanner is another type of 3D depth sensor for non-contact measurement applications including quality inspection, prototyping, reverse engineering, and 3D modeling. Compared with 3D structured light cameras, laser profile scanner projects a laser line onto the subject at a high frequency and either uses a triangulation process with a camera or uses reflection time to calculate the depth data. A 3D depth profile can be created depending on the subject's moving speed. It has the advantages of high measuring accuracy and high scanning frequency than previous two 3D sensors. In this section, three different laser profile scanners (SICK LMS400-2000, Acuity 820–1000, and Gocator 2380) were tested and evaluated to analyze their potential application for the cuttings/cavings monitoring project.

SICK LMS400-2000

SICK LMS400-2000 emits an infrared laser beam to subject and generates the depth data based on the principle of phase shift (ToF). The phase difference is calculated based on the propagation time of the light and the wavelength difference between emitted beam and received beam due to phase shift. Later, a frequency is converted based on the phase difference and it generates the distance to the object (SICK, LMS400 Laser measurement sensor 2013). This sensor is designed to generate 3D profile of the object on a manufacturing conveyor belt with known input moving speed.

Figure 5-6: SICK LMS400-2000 laser scanner (left) and field of view (right) (SICK, LMS400-2000 Data Sheet 2012)

The LMS400-2000 has dimensions of 179 mm x 107 mm x 130 mm (L x W x H). It has a scanning frequency of 270 Hz to 500 Hz and a configurable angular resolution from 0.1° – 1.0 °. It emits visible red light with 650 nm wavelength and is powered by 24 V DC. As shown in Figure 5-6, the sensor can cover a wide range of measurement up to 3.44m. The ambient operating temperature is 0° to 40°C (32° to 104°F). Figure 5-7 illustrates how the measurement is performed on a conveyor system (SICK, LMS400-2000 Data Sheet 2012).
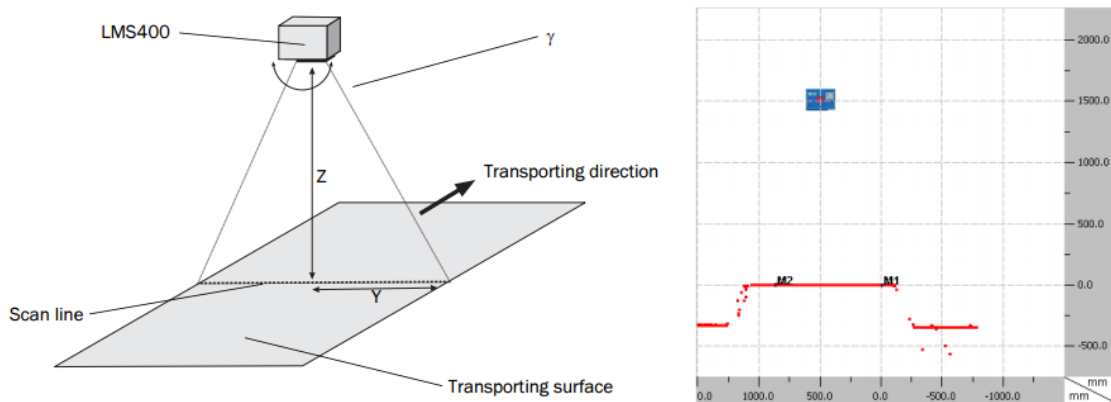
Figure 5-7: Y coordinate and z coordinate (left) and scanned conveyor system (right) (SICK, LMS400 Laser measurement sensor 2013)

44

The ambient lighting environment less affects LMS400-2000. A demo testing was performed in the laboratory. The sensor was placed 1 meter directly above the static cuttings sample. However, the sensor was not able to generate an accurate line profile of cuttings. The measured signal was noisy and failed to capture rock samples smaller than 3 mm.

Acuity 820–1000

Acuity AccuProfile 820-1000 2D laser scanner has two sensors: a laser beam emitter and a CCD image sensor. To acquire surface height profiles, a beam of visible laser light (658 nm wavelength) is projected on the target surface. By using the triangulation method, a CCD detector examines reflected light from the subject at a fixed angle. The laser sensor scans 500 data point at each 2D line scan with a frequency up to 100 Hz. The 2D contour profile data is then transmitted to a computer via Ethernet cable. It uses a 10-30 VDC power source. Based on the object moving speed, 3D profile can be generated to calculate the volume of the scanned object. The measuring range is from 550 mm to 1550mm in the z-direction is and 500 mm to 800 mm in the x-direction. Respectively, the resolution in z and x directions is 630 μm. Acuity 820-1000 sensor has physical dimensions of 1150 mm x 32 mm x 60 mm (L x W x H), which makes the sensor quite lager in length (as shown in Figure 5-8). The working environment is 0° to 40°C (32° to 104°F) with cooling option up to 400°C (752°F). (Acuity, AccuProfile 820 Laser Scanners User's Manual 2013)
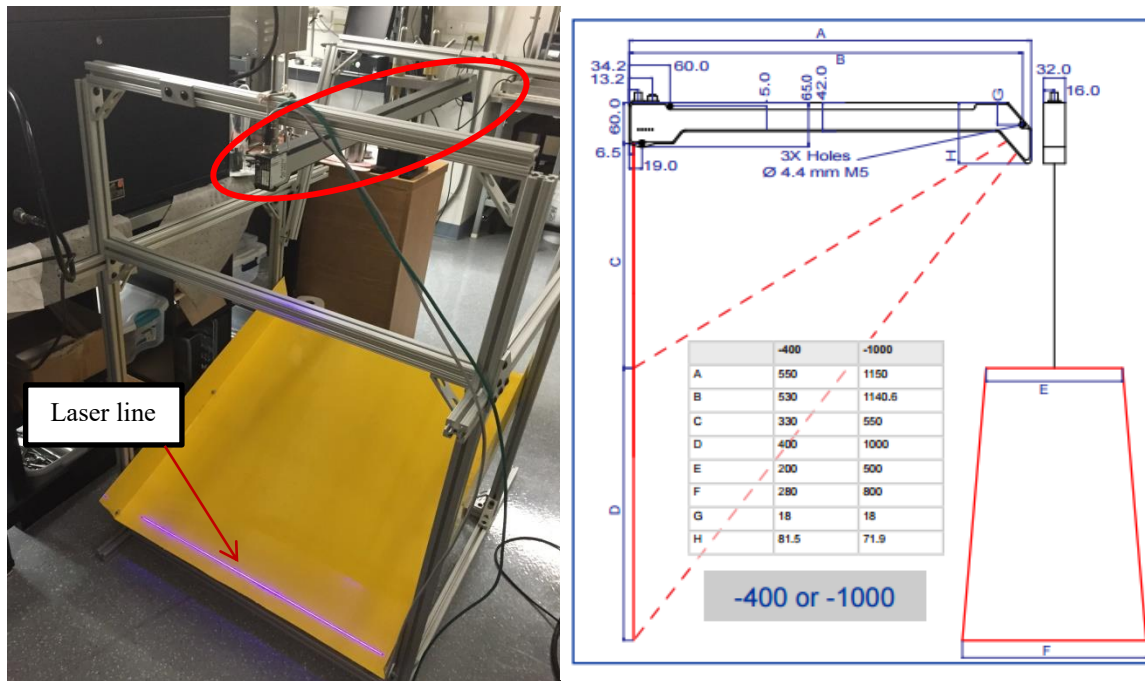
Figure 5-8: AccuProfile 820 2D laser scanner circle in red (left) and 820-1000 model dimensions (right) (Acuity, The AccuProfile 820 2012)

To test the measurement of Acuity 820-1000 laser scanner, the sensor is mounted on aluminum frame structure as shown in Figure 5-8. A 36 inches wide yellow ramp is placed below the sensor at a tilted angle parallel the laser scanner. The vertical distance is kept as 1.2 meters in order to allow the laser beam to cover the whole ramp. The drilling cuttings were placed static on the laser line and a 2D profile was produced to represent the height of cuttings as shown in Figure 5-9. The drillings cuttings were collected from the field and had a composition of 70 % shale and 30% sandstone. Based on this laboratory test, Acuity 820-1000 laser scanner proves to have an accuracy of 1 mm in both z and x directions. By utilizing manufacture software, the system can reconstruct a 3D profile as shown in Figure 5-10 for demonstration. Since the cuttings were not moving in this case, the profile is just a cross-section of the cuttings pile. Later, the volume of cuttings can be calculated based on the retrieved 3D depth data. AP820 laser scanner uses Windows

dynamic link library (DLL) for calling functions to start measurement and collect results. With full manufacture SDK, it is feasible to program the sensor to perform measurement in C++ or Visual Basic (VB) DotNet environment.
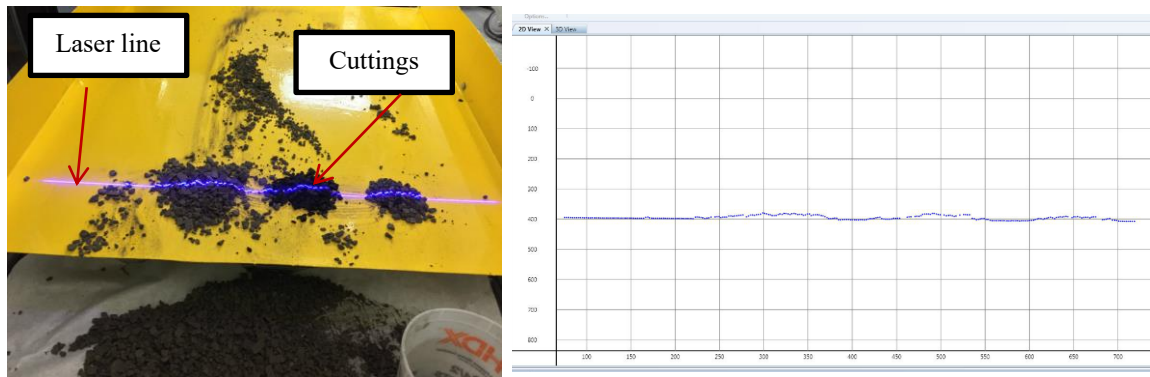
Figure 5-9: AccuProfile 820 2D laser sample scan over fresh cuttings (left) and 2D depth profile of cuttings (right).
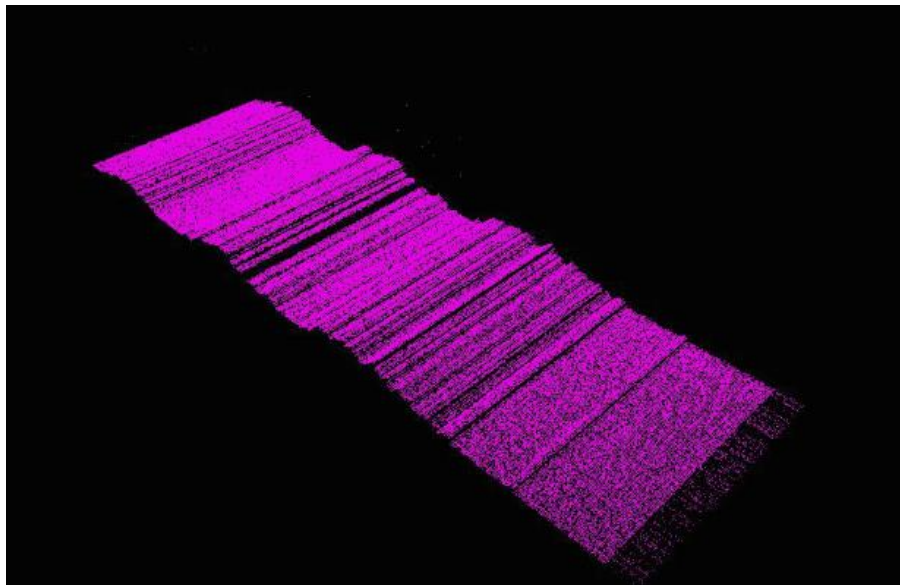
Figure 5-10: 3D profile of static drilling cuttings by AccuProfile 820 2D laser scanner

Gocator 2380

Gocator 2380 is a smart 3D profile scanner designed by LMI Technology Company. Similar to Acuity 820-8000 laser profile scanner, Gocator profile sensor emits a laser line to measure cross-sectional shapes of parts and materials surfaces. The device is designed to inspect product quality for automotive, automation, and other industry solutions. Gocator 2380 has two sensors in the camera. A laser emits structured light for laser profiling and a camera observes laser light reflected from target surfaces at a certain angle. This triangulation angle allows the camera to measure laser line in different positions. The wavelength of the laser source is 660 nm. Gocator 2380 sensor scans 1280 data points at approximately 170 Hz to 5000 Hz. It requires a 24 to 48 VDC input voltage. The measuring range is from 350 mm to 800 mm in z-direction and 390 mm to 1260 mm in x-direction (FOV) as shown in Figure 5-11. Based on the measuring range, the z-resolution is from 0.092 mm to 0.488mm and x resolution is from 0.375 mm to 1.100 mm respectively. This laser sensor has a compact gasket aluminum enclosure with dimensions of 272 mm x 49 mm x 75 mm (L x W x H) (T. LMI 2016). Gocator 2380 sensor is suitable for operation between 0 – 50°C and 25 – 85% relative humidity (noncondensing). A connector, Master 100, is used to provide power, trigger input and encoder to the Gocator 2380 sensor. It can be considered as a safety switch. A gigabit Ethernet cable is applied to control the sensor from a computer and transmit measured data. The sensor also has a browser-based configuration and open source SDK to allow the user to control the sensor and perform real-time 3D visualization (as shown in Figure 5-12). The open source SDK is available in C++, C sharp, and VB programming environment. It allows the user to manipulate the code to control Gocator laser scanner without using its browser-based user interface (UI). The browser-based UI has limited functionality and compatibility for other software.
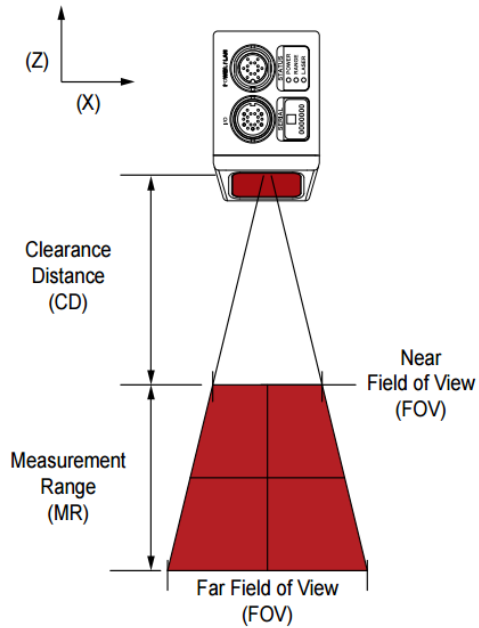
Figure 5-11: Gocator 2380 and Master 100 Connector (left); Sensor FOV(Right) (T. LMI 2016)

To test the performance of Gocator 2380 laser scanner, two experiments were performed for both static and dynamic targets. For the static accuracy test, the sensor was placed 1.2 meters vertically from cuttings sample as shown in Figure 5-12. Cuttings sizes were ranging from 2 mm to 20 mm. Figure 5-13 shows the scanned profile of some small cuttings. It demonstrated that the sensor managed to capture the depth profile of cuttings down to 1 mm to 2mm in size.
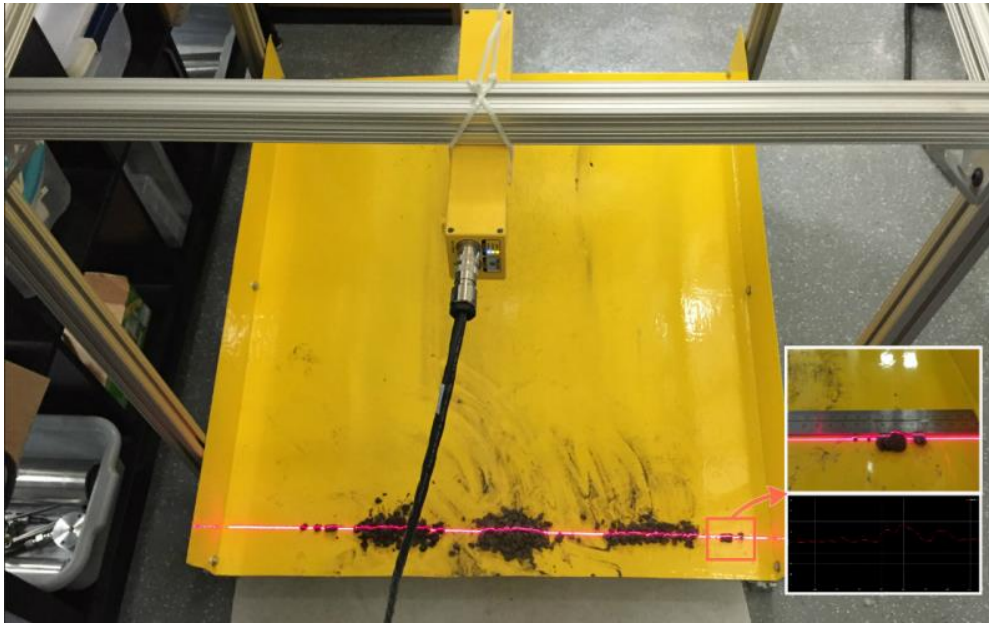
Figure 5-12 Gocator 2380 testing set up
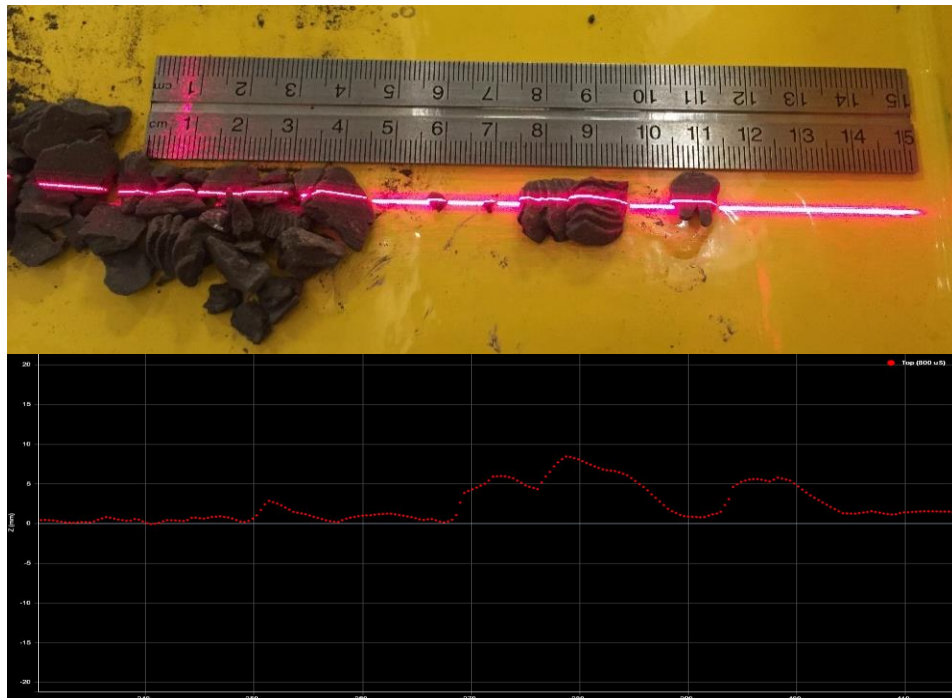
Figure 5-13: Cuttings scan and 2D profile.

50

Furthermore, to validate the performance of the sensor in motion, the sensor was brought to the University of Texas at Austin Nuclear & Applied Robotics Laboratory where a robotic arm could grasp the laser sensor to perform the linear motion. The purpose of this test was to imitate a scenario when cuttings were moving/sliding down on the yellow ramp. As shown in Figure 5-14, the sensor was held 1 meter above some cuttings sample. The robotic arm manipulator moved in the y-direction at a constant speed: 500 mm/s. After the scan finished, Gocator browser-based UI was used to generate a 3D profile of cuttings. However, it took about 2-3 seconds for rendering which generated a 3D image of the cuttings (as shown in Figure 5-15 left). The volume of the sample was also calculated by built-in SDK as 54.7 ml. Laster, a measuring cylinder (Figure 5-15 right) was applied to measure the exact volume of 43.6 ml. The error percentage was 25% compared to the actual volume. The irregular shape of cuttings mainly caused this volume difference. The laser scanner only scanned surfaces of cuttings. When performing volume measurement, void space below cuttings was also included in the calculation (shown as the dark/shaded area in Figure 5-15 left). Nevertheless, Gocator 2380 demonstrates to have high accuracy in both z and x directions. The generated 2D profile data can be used to plot a 3D profile of the target.
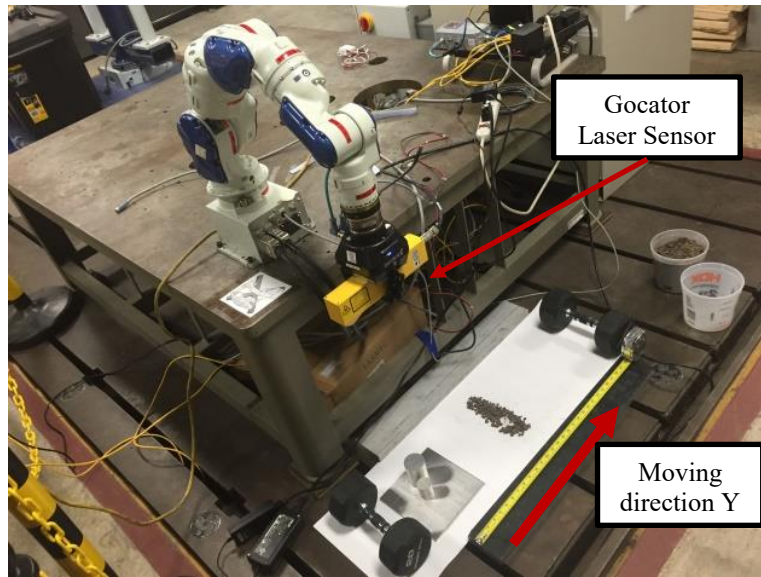
Figure 5-14: Gocator 2380 mounted on a robotic arm
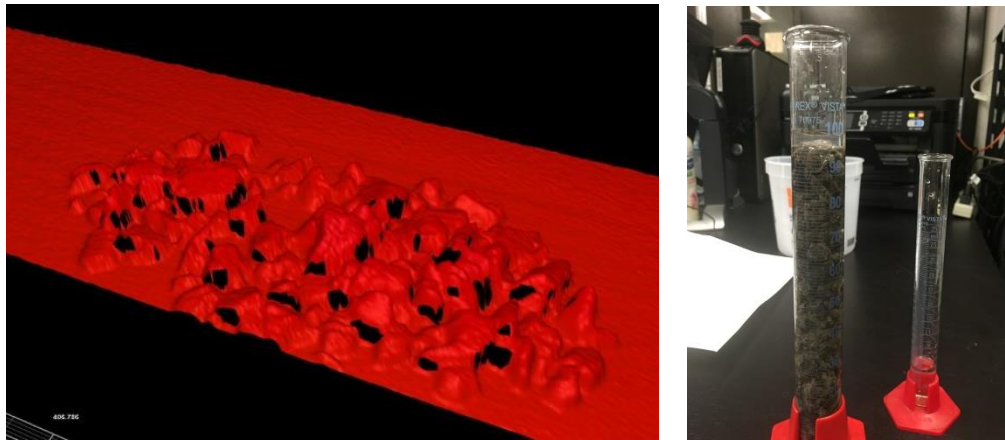
Figure 5-15: 3D profile of scanned cuttings (left) and volume measurement (right)

5.1.3 Sensor Selection Summary

In the previous two sections, it provided an overview of commercially available 3D structured light cameras and 2D/3D laser profile scanners. Each sensor was evaluated and tested upon their feasibility for cuttings real-time measurement. Both vision systems can

be used to quantify cuttings/cavings volume and generate a 3D profile of measuring target. Sensors were evaluated based on their advantages and disadvantages with regard to field of view, measuring speed, accuracy, cost, and ambient lighting environment performance. A brief evaluation of each sensor is presented in Table 5-2. Even though it is difficult to find a perfect solution to satisfy all design requirements, we can narrow down the sensor selection based on their performance. The benefit of 3D structured light cameras is to take a snapshot of the measuring target and generate 3D depth profile. However, with respect to the field of view and accuracy, current commercial 3D structured light cameras do not prove to have enough resolution and are strongly affected by ambient lighting condition. In addition, the scanning frequency of sensors might not be suitable to monitor moving cuttings. On the other hand, laser profile scanners are able to cover a large scanning range and have a higher resolution down to 1mm in both horizontal and vertical directions. Although laser profile scanner only provides a 2D profile of target surface, with accurate moving speed input, its high-frequency depth data can be reconstructed by computer vision technique to measure target volume and produce a 3D depth profile. In order to achieve desired resolution, the selection can be narrowed down to Acuity 820-1000 laser scanner and Gocator 2380 laser scanner. As evidenced in the laboratory testing, Gocator 2380 smart profile scanner was proven the most suitable selection to meet all possible criteria. The advantages of this sensor are compact, large FOV, high accuracy, and relatively lower cost. It should be kept in mind that the hardware of this sensor is not specifically designed for oil and gas industry application. A proper enclosure can be used to protect sensors in hazardous outdoor environment. Details of sensor enclosure will be discussed in Chapter 6. In conclusion, Gocator 2380 smart laser scanner is selected to depth data of cuttings. In order to measure moving cuttings volume and properties, a unique 2D and 3D combined vision system will beproposed and detailed in the later sections of this chapter.

Table 5-2: Conclusion of five 3D depth sensors

	Kinect 3D Sensor	ENSENSON20	SICK LMS400-2000	Acuity 820 – 1000	Gocator-2380
Type	Structured Light	Structured Light	Laser	Laser	Laser
Scanning Frequency	Slow	Slow	High	High	High
X an Z resolutions	Low	Low	Medium	High	High
Meet FOV Requirement	YES	NO	YES	YES	YES
Size	Compact	Compact	Compact	Large	Compact
Cost	$150	$15,000	$7,379	$15,575	$10,770 $6,848 (Demo)

5.2 INTEGRATED 2D AND 3D VISION SYSTEM DESIGN

As discussed in Section 3.1, Gocator 2380 profile laser scanner is selected to measure the depth profile of cuttings. However, without determining cuttings moving speed, a detailed 3D profile cannot be produced. In this section, an integrated 2D and 3D computer vision system is designed aiming to extend existing technology to accurately measure cuttings/cavings volume, size, and shape in real-time. By using the image

processing technique, a 2D HD Camera was added to measure cuttings moving speed and analyze size distribution of cuttings. With the synchronization of measured cuttings speed and 2D laser scanning frequency, a 3D profile of cuttings can be generated and volume can be determined.

5.2.1 System Physical Design

The best location to monitor cuttings is over the cuttings ramp where cuttings slide down the ramp into a collecting pit at a relatively steady speed. In order to capture cuttings/cavings properties, a proposed location for the installation of sensors is under the shale shaker floor and above the ramp (as illustrated in Figure 5-16). The benefit of this design is that the system can avoid the vibration and drilling fluid splash above the floor. Figure 5-16 displays a proposed layout of the system. After drilling fluid is filtered out by shale shake system, wet cuttings drop by gravity onto a ramp and slide into a collecting pit. As cuttings sliding down the tilted ramp, cuttings speed achieves steady state the then bottom end of the ramp due to drilling fluid' presence and friction. This creates a desired environment to measure cuttings speed and calculate cuttings volume.
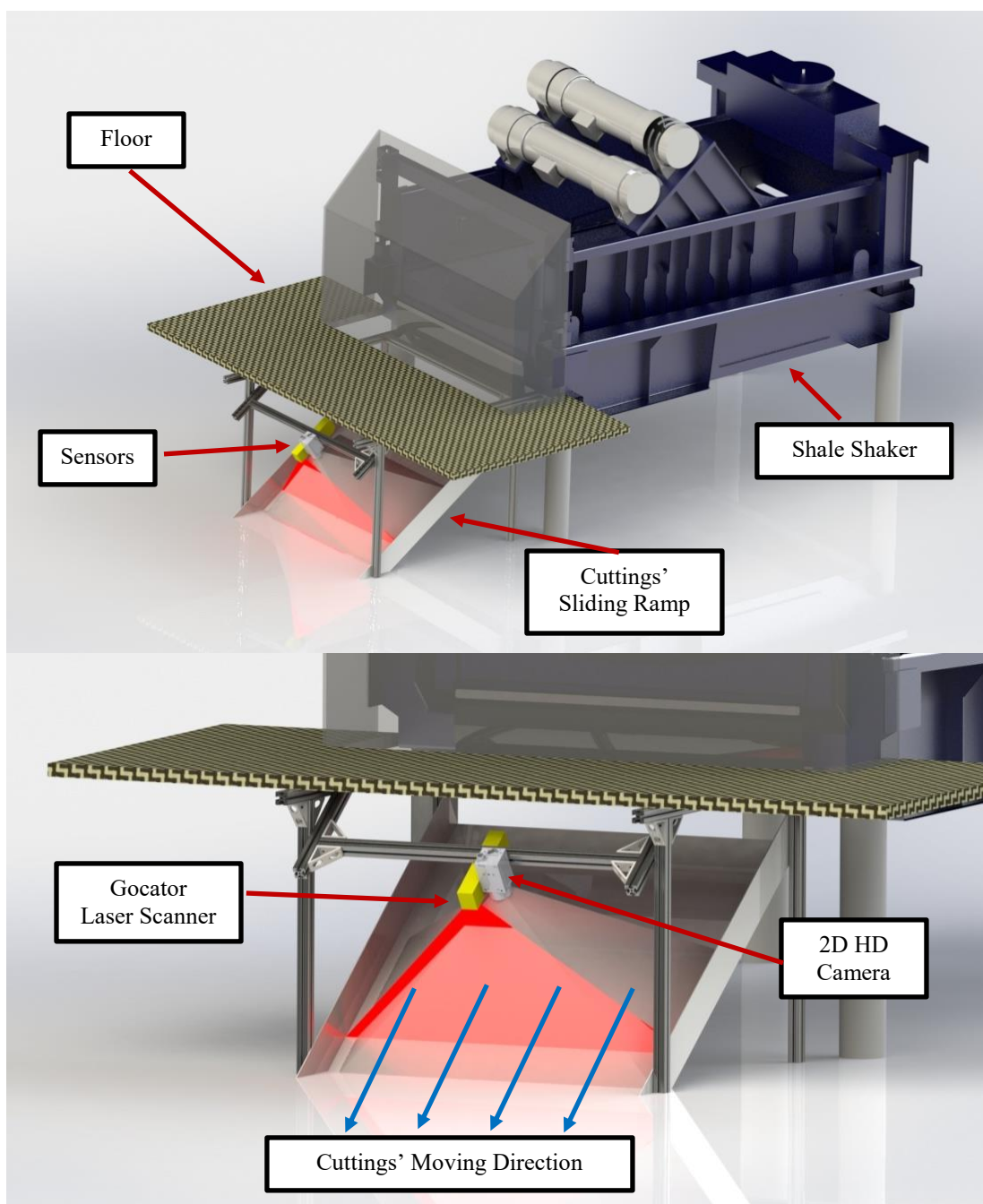
Figure 5-16: UT Austin Cuttings Monitoring Testbed Design

The testbed was then constructed in the laboratory. The frames were made of 80/20 aluminum beams. A yellow steel ramp was installed at an adjustable angle to intimidate

the cuttings ramp on a drilling rig. The frames have dimensions of 48 inches x 36 inches x 48 inches (L x W x H). The yellow ramp is 36 inches wide and the tilted angle can be adjusted from 0 to 75 degrees. As shown in Figure 5-17, Gocator laser scanner (yellow sensor) and 2D HD camera (black sensor) were mounted parallel to the ramp. This design allows changing measuring distance and ramp' angle.
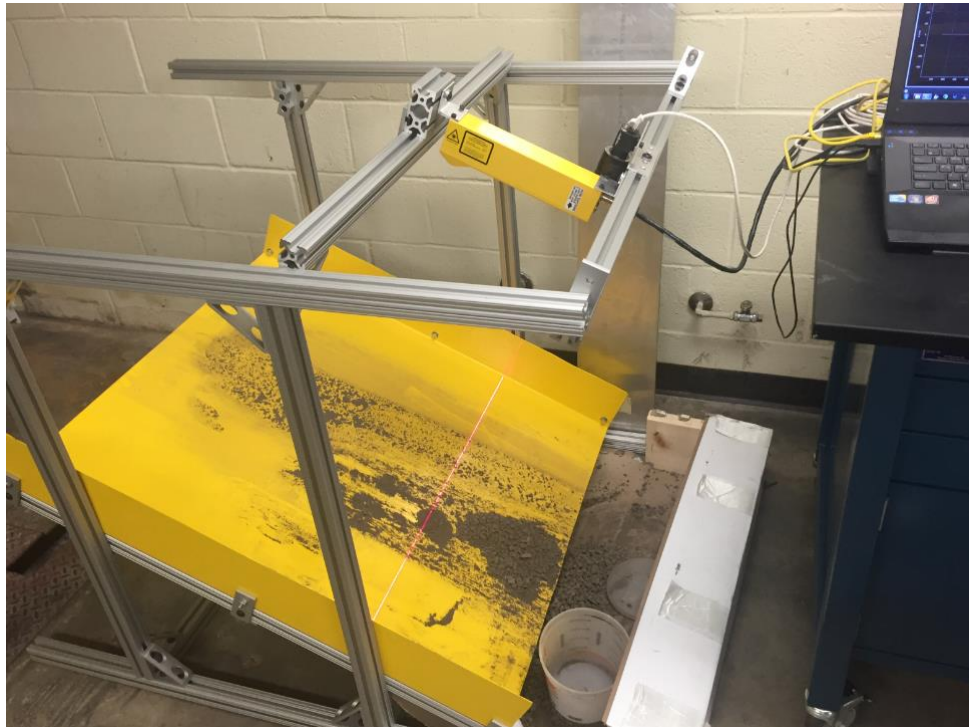
Figure 5-17: UT Austin Cuttings Monitoring Testbed

5.2.2 2D HD Camera and 3D Laser Scanner Electrical Hardware Design

This section presents a description of electronic devices used in the system. An understanding of all components builds the foundation for measurement, data transmission, and system communication logic. Figure 5-18 shows the devices in the system. Table 5-3 table lists some key specifications and description of the components.
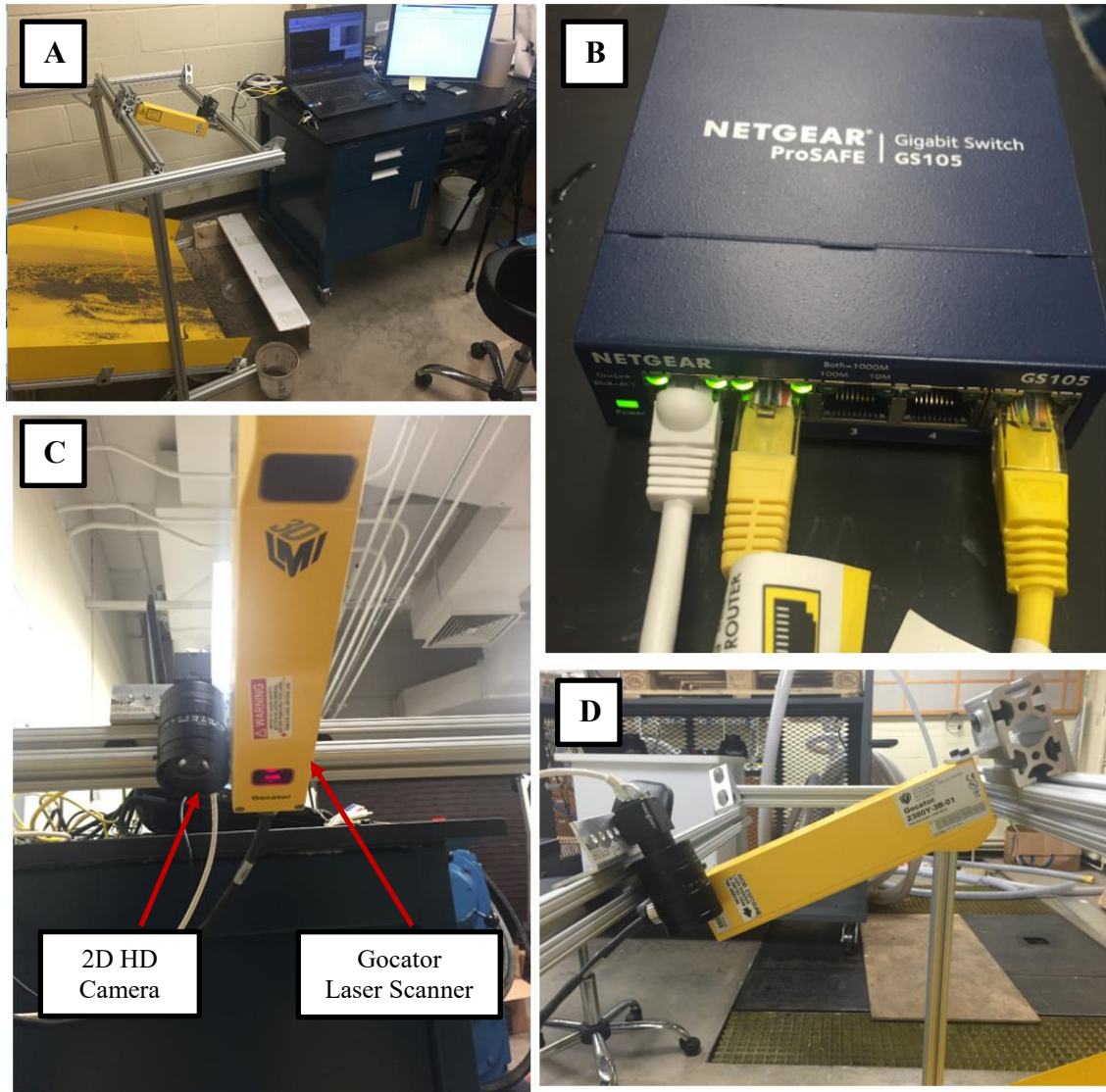
Figure 5-18: Electrical components of the design; A) Laboratory setup, B) Ethernet switch, C) Bottom view of 2D camera and laser scanner, and D) Side view of 2D camera and laser scanner

Table 5-3: Summary of electric devices

Items	Specification and description	Power Source
Gocator 2380 Laser Scanner	• High-frequency 2D profile scan • Generate 3D depth data • Data is transmitted via Ethernet	24 to 48 VDC
Point Grey Black Fly Camera	• High resolution image capture • For cuttings moving speed measurement • For cuttings size distribution analysis • Data is transmitted via Ethernet	56 V PoE
NETGEAR Gigabit Ethernet Switch	• Gigabit Ethernet switch for connection terminal	12 V
Category 6 Ethernet Cable	• Up to 100 meters at 500 MHz	N/A
Computer	• Control laser scanner and 2D HD camera • Run computer vision algorithms to calculate cuttings speed, volume, and size distribution.	110 V

2D HD Camera

The unique design of this integrated 2D and 3D computer vision system is to include a 2D camera to measure cuttings moving speed. Point Grey Blackfly 2.3MP Color GigE PoE camera was selected to capture high-resolution images at high speeds. This model leverages Sony's Pregius global shutter CMOS technology to generate a crisp and clear image for high-speed image capturing. It has a resolution of 1920 x 1200 at 41 fps

and generates 2.3 megapixels (MP) image (PointGrey, Blackfly 2.3 MP Color GigE PoE (Sony Pregius IMX249) 2015). The sensor is lightweight and compact (30 mm x 29 mm x 29 mm L x W x H). A RoHS Fujinon 12.5 mm fixed focal length lens is used to adjust the focus of the camera (as shown in Figure 5-19). Image data is transmitted via Ethernet cable. The advantage is long-range data transmission and low cost. Point Grey also provides open source SDK to allow the user to customize camera's resolution, color, and frequency. This is important to this project because certain features affect computer vision calculation speeds.

Figure 5-19: Point Grey Blackfly HD Camera (30 mm in length) and Fujinon Lens (70mm in length)

NETGEAR Gigabit Ethernet Switch and Ethernet Cable

The PoE data transmission method is chosen to allow remote control over the sensors at the field testing. Category 6 Ethernet cable transmits 10 Gigabit data up to 500 Mhz (Barnett, Groth and McBee 2004). Since this application requires rich depth data and high-resolution image transmission, Category 6 Ethernet cable is an ideal choice. An Ethernet switch is then used to connect both Gocator laser scanner and Point Grey HD camera to a computer.

5.3 REAL-TIME COMPUTER VISION SYSTEM ALGORITHM AND SOFTWARE DESIGN

As discussed in Chapter 3, computer vision techniques are widely used in manufacturing industry for volume measurement and quality inspection. In the mining industry, a laser scanner is used to quantify coals on a conveyor belt. [REF] A similar technique can be applied here to monitor drilling cuttings and provide more information to reflect drilling performance. One major challenge in this application is that a conveyor belt system does not present on a land drilling rig. Adding a conveyor belt will increase the complication of the shale shaker system, which might cause downtime of drilling operations because of maintenance or malfunction.   Therefore, the speed is an unknown input parameter and cannot be used either calculate the target's volume or generate a 3D profile. Fortunately, drilling cuttings return to a collection tank by sliding down a ramp with gravity. Cuttings appear to move at a steady speed with a small presence of drilling fluid. This makes it possible to use machine vision techniques for calculating how fast the cuttings are moving. Then, the measured speed can be used as an input for 3D profile modeling and volume calculation. This section first presents the computer algorithms on how to real-time calculate: (1) cuttings moving speed, (2) cuttings volume, and (3) cuttings size distribution. Then a system logic map is drawn to illustrate how information is

communicated between sensors and computer terminal. Due to the limitations of built-in manufacture software of each sensor, the provided software cannot be used to perform all required measurement. Gocator 2380 and Point Grey 2D camera open source SDK libraries are applied to program the measuring algorithms in Microsoft Developer Tools – Visual Studio.

5.3.1 2D Cuttings Speed Tracking

The purpose to measure cuttings moving speed is to negate the need for a conveyor belt, which provides fixed speed input via an encoder. In this section, adaptive background subtraction technique is applied to calculate the binarized difference between frames. By analyzing the binarized difference, speed information can be retrieved based on known camera frame rate. The program is written in Microsoft Visual Studio in C++ programming language. Point Grey FlyCapture SDK (PointGrey, FlyCapture SDK 2016) is implemented in the program to control and acquire images from Point Grey GigE Blackfly camera. The main functions used are image grabbing and image format converting. In the meanwhile, Open Source Computer Vision (OpenCV) SDK is applied for background subtraction, centroid calculation, and some other basic image processing techniques (OpenCV 2016). Detailed calculation algorithm is as followings:

1. Point Grey GigE Blackfly camera is triggered and calibrated at a fixed frame rate: 30 fps

2. Three successive images (frame_1, frame_2, and frame_3) are grabbed in sequence as the cuttings sliding down the yellow ramp (as shown in Figure 5-20).

3. Images are converted by FlyCapture SDK into OpenCV Mat format (OpenCV 2016) in order to be processed by OpenCV functions.

4. Functions like, *cvColor*, *absdiff*, *threshold*, and *erode* from OpenCV are used to preprocess the image to greyscale with a certain threshold.

5. *cv2.createBackgroundSubtractorMOG()* (OpenCV 2016) is then applied extract the moving objects the previous frame. As shown in Figure 5-21, Figure 5-21A is the binarized difference between frame_2 and frame_3 while Figure 5-21B is the binarized difference between frame_2 and frame_1.

6. Then each frame is cropped into five small fractions along the laser line as demonstrated in Figure 5-21 C & D. There are a few benefits to analyze smaller image: a) more steady cuttings moving speed at the end of the ramp; and b) faster processing speed.

7. In each cropped image like Figure 5-21C. the pixels are segmented into five event columns. In each column, the centroid of each white cluster is calculated by functions like: *findContours()* and *computeCentroid()* (OpenCV 2016). To reduce error, abnormally small or large clusters are not calculated.

8. By comparing the pixel position of each centroid in the respective column between two images (Figure 5-21 C and D), the moving speed of cuttings is calculated. The unit of the speed is in pixels. Knowing the exact distance between the yellow ramp and camera lens, captured image is pre-calibrated as 1 pixel = δ mm.

   a. Center coordinates of Clusters a_i and $a\_(i-1)$ are (X_i, Y_i) and (X_j, Y_j) in pixels

   b. $v = (Y_j - Y_i) \times \delta \times 30$ mm/s

9. Along the laser line, there are 5 x 5 = 25 columns and calculated 25 moving speeds. The average speed is then finalized by filtering out abnormal values and averaging the rest.

10. Save speed value.

11. The process is repeated from Step 2 for another set of frames.

This algorithm allows direct and fast speed measurement by background subtraction method. The resulting speed is passed into another part of the program for volumetric measurement, which will be discussed in next section.
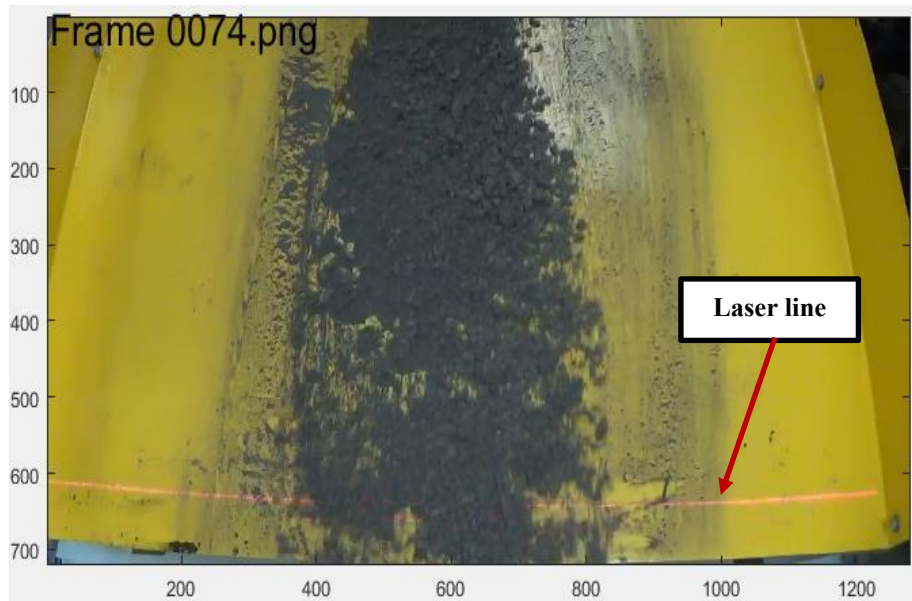
Figure 5-20: High resolution streaming of moving cuttings.
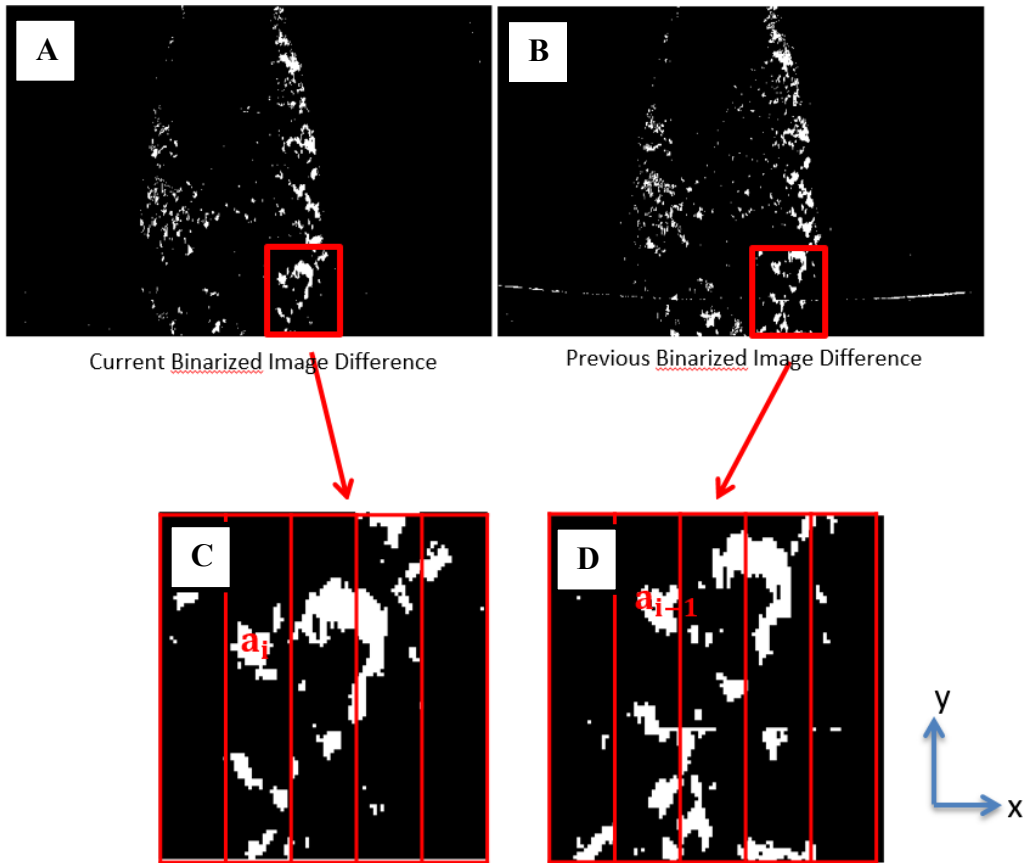
Figure 5-21: Adaptive background subtraction (A & B) and speed measurement (C & D)

5.3.2 Cuttings Volume Measurement and 3D Profile Reconstruction

Gocator 2380 laser scanner only provides high-frequency profile scan over the cuttings surface. To successfully calculate the volume of cuttings and build a 3D depth profile, calculated cuttings moving speed is synchronized with laser scanning frequency. The browser-based Gocator software cannot be reprogramed to use calculated cuttings speed. Therefore, in Microsoft Visual Studio, Gocator SDK (LMI 2016) is used to retrieve raw 2D profile depth data for volume calculation. To generate a 3D model of the scanned target, Windows build-in Microsoft Direct3D 9.0 Graphics SDK (Microsoft, Classic

DirectX Graphics 2016)is implemented in Visual Studio to plot the profile. Detailed calculation algorithm is as followings:

1. Browser-based Gocator software is used for calibration. The scanning frequency is set as 100 Hz.

2. The program is opened in Visual Studio to trigger Point Grey 2D HD camera for speed measurement and Gocator laser scanner for raw profile depth data.

3. Both functions are running at the same time.

4. Once the raw 2D profile data is received (as shown in Figure 5-22). The each red data point has two coordinates: x and z in mm. For example:

    a. Adjacent two dots: a_i and a_j have coordinates of (x_i,z_i) and (x_j,z_j).

    b. The area covered by two dots can be calculated as a trapezoid:
    $$Area_c = (x_j - x_i) \times (z_j + z_i)/2$$

5. The volume of each line scan is then calculated based on cuttings moving speed v:
    $$unit\_Volume = v \times Area_c/100 \ (mm^3 \ per \ scan)$$

6. The final volume of the scanned target is $unit_{Volume} \times number of \ scans$

7. This calculated volume includes the void space covered by the top surfaces of the target. To improve the measurement, a experiment was performed to finalize a confident ratio to use as a correction threshold.

8. The actual volume of cuttings = scanned volume $\times$ (1 - void ratio).

9. Direct3D library allows to real-time generate a 2d/3D visualization of the measured target as shown in Figure 5-23 (a 3D profile of a hand moving across the laser line). The color from green to red represents the height of the target from high to low.

10. Gocator browser-based software is able to off-line produce a rendered 3D profile as shown in Figure 5-24 (a 3D profile of cuttings sliding down the ramp). However, this rendering process took about 2-3 seconds to generate the 3D depth profile. The color range indicates the height of cuttings.
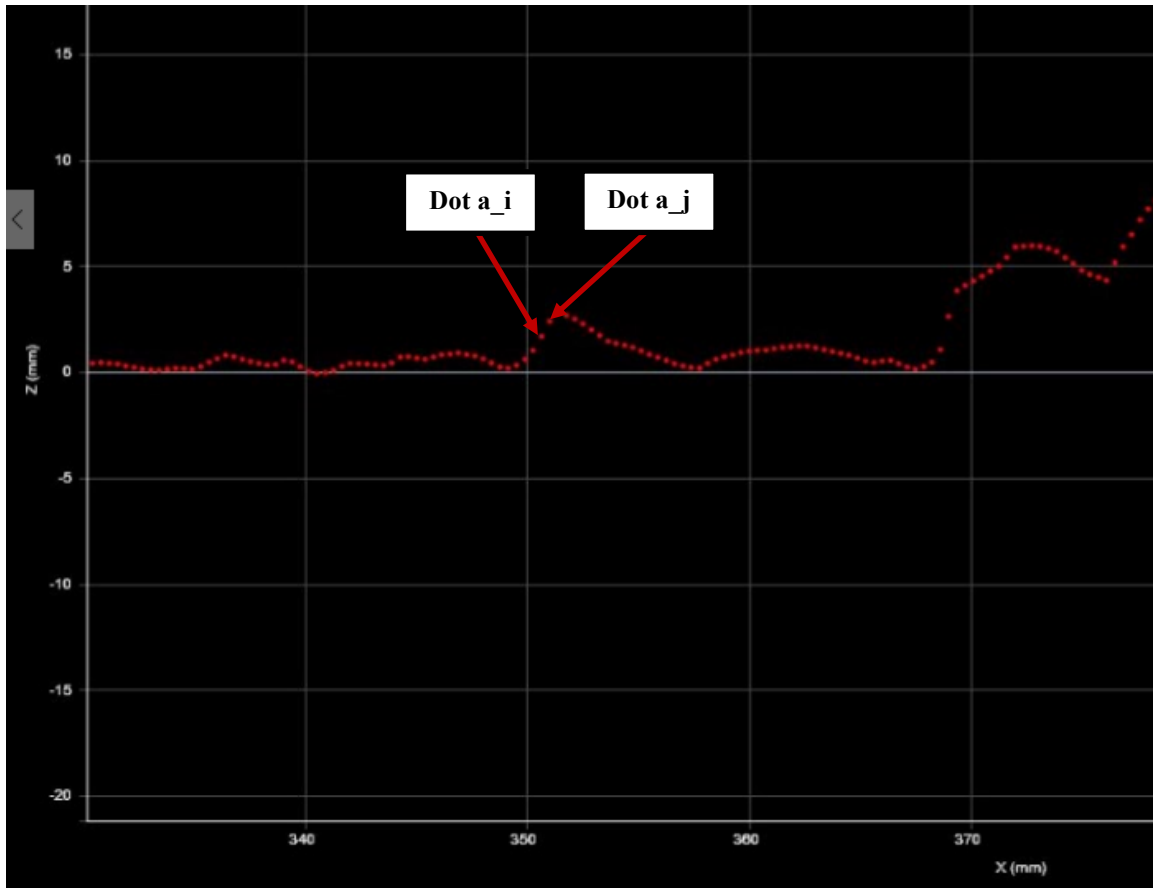
Figure 5-22: Demonstration of cross section area calculation
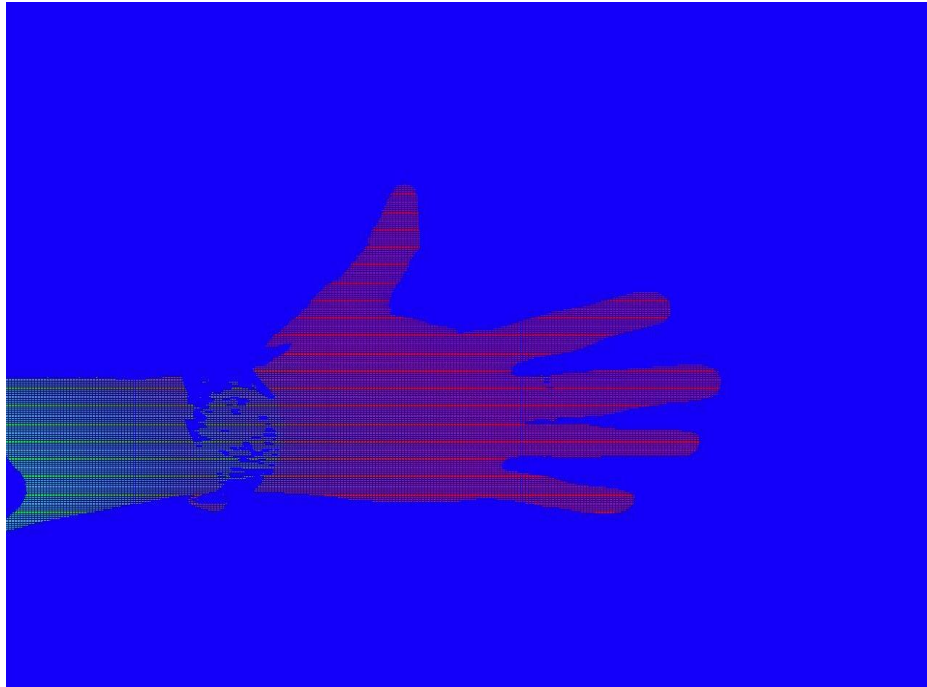
Figure 5-23: A generated 3D profile from 2D laser data based on Direct3D library
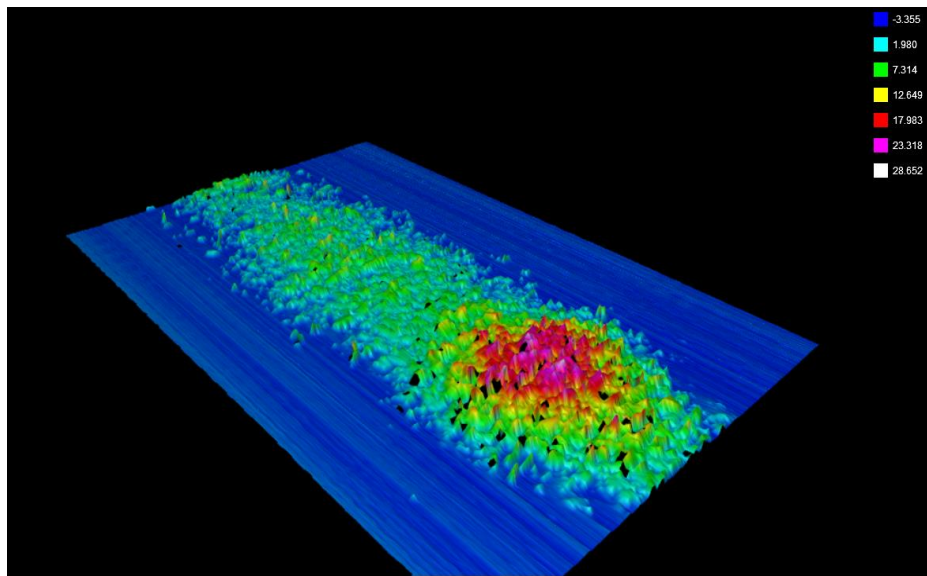
Figure 5-24: A generated 3D profile of moving cuttings from 2D laser data collected as showing Figure 5-22.(in mm).5.3.3 Cuttings Size Distribution Analysis

Drilling cuttings represent the lithology being drilling in a wellbore. The size range indicates may indicate the performance of drilling bit, drilling parameters, mud properties, and hole cleaning efficiency. As reviewed in Chapter 3, there are various edge detection methods. For the first attempt, a digital image was captured by Point Grey HD camera at a resolution of 1920 x 1080. The lighting condition was the regular indoor environment. Canny edge detection method is applied through OpenCV library. OpenCV function: *Canny(InputArray **image**, OutputArray **edges**, double **threshold1**, double **threshold2**, int **apertureSize**=3, bool **L2gradient**=false)* was used to determine the edges of cuttings. The properties described by each function can referred to OpenCV library (OpenCV 2016).

With some adjustment of noise level and threshold value, the majority of cuttings were differentiated from the background environment as shown in Figure 5-25. With the help of edge detection, cuttings were presented as contours in the image. Contours have the same color or intensity and can be represented by a curve joining all the continuous points along the boundary (Maire 2009). The detected contours can be used to calculate the size of each cutting. The detailed procedure is as followings:

1. Visual Studio triggers Point Grey Blackfly camera and an 1920 x 1080 image is captured.
2. FlyCapture SDK is applied to convert the image format to OpenCV Mat.
3. *Canny()* edge detection is applied to find the edges of cuttings (Figure 5-25)
4. *findContours()* algorithm is implemented to retrieves contours from the binary image (OpenCV 2016).
5. *counterArea()* function is used to calculate pixel area of each contour/cutting (OpenCV 2016)
6. Area of each contour is converted to unit mm^2 based on pre-calibrated scale: 1 pixel $= \delta$ mm.

7. Cuttings are estimated as circle. Then the diameter is calculated as:

$$r = \sqrt{\frac{Area}{\pi}}\ mm$$

8. A size distribution of cuttings is plotted as shown in Figure 3-26

*Note: this is a preliminary test for cuttings size distribution measurement. Intense processor loading is observed. The processing time takes about 10 to 50 seconds depending on the level of details in the image. The success of the algorithm also heavily depends on the lighting environment and adjustment of *Canny* threshold value. This algorithm proposes a feasible machine vision technique to quantify cuttings size distribution. Future work is required in order to justify the measurement based on field trial in different lighting environment.
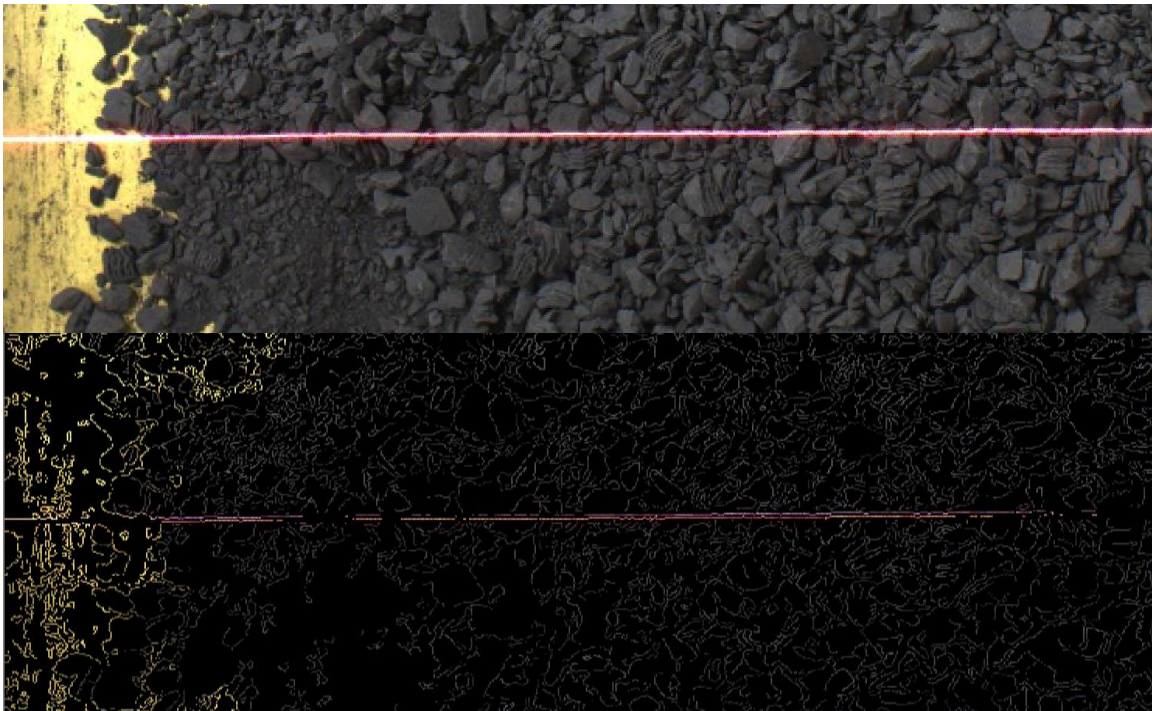
Figure 5-25: Original image (upper) and processed image (lower) by Canny edge
        detector.
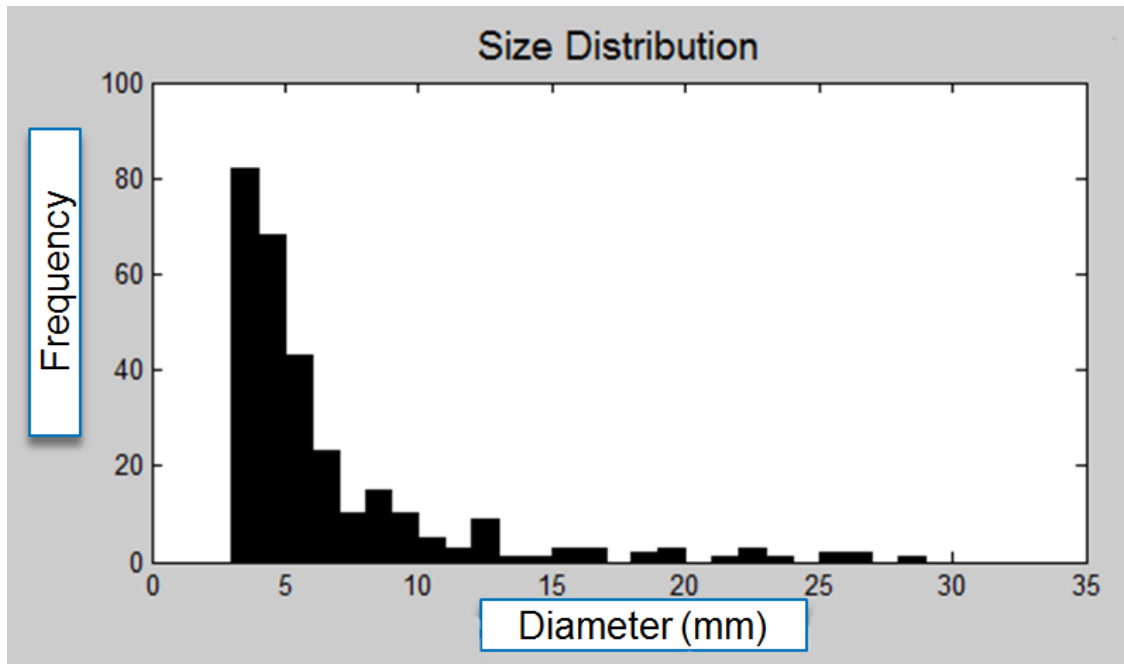
Figure 5-26: Cuttings size distribution

5.3.4 Software Design and System Logic Map

As described in the previous three sections, different computer vision techniques were applied to measure cuttings moving speed, volume, and size distribution. In order to design a real-time cuttings monitoring system, Visual Studio C++ language is selected as the programming environment. Visual Studio allows controlling Gocater 2380 laser scanner and Point Grey Blackfly HD camera at the same.Concurrently, opens source SDK libraries of each sensor can be added into Visual Studio together with OpenCV and Direct 3D imaging processing libraries. A software interface is shown in Figure 5-27. Measured cuttings moving speed and volume are displaced in the Window console. In the meanwhile,

71

the blue window is a display for remonstrated 3D profile of cuttings.   The bottom image
is used for speed measurement and real-time streaming.
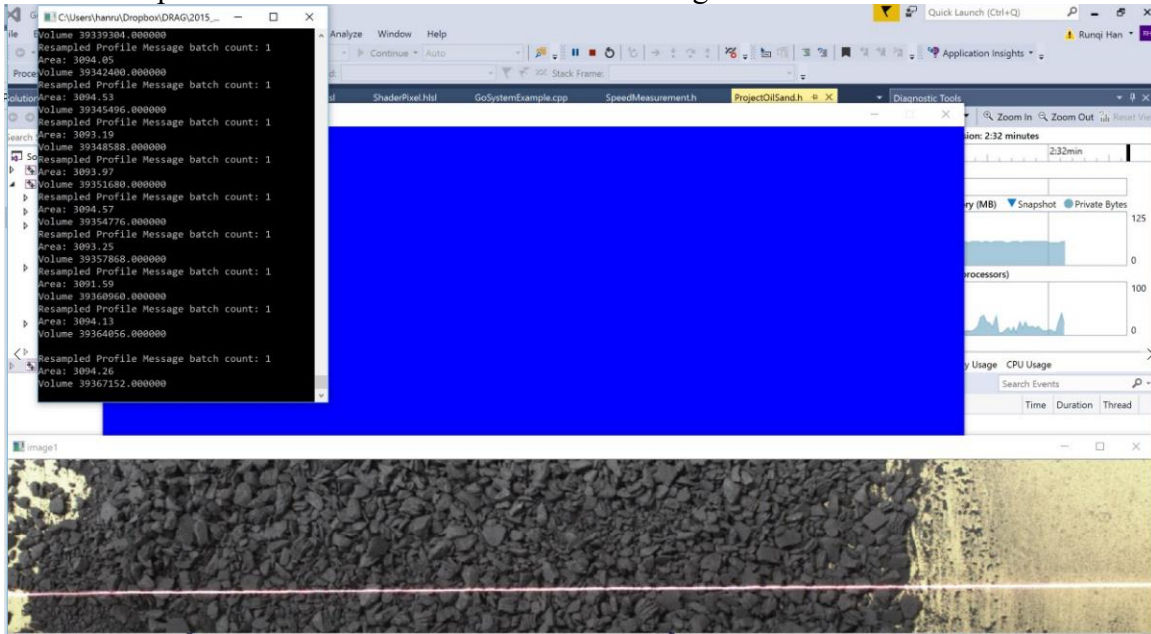
Figure 5-27: Visual Studio 2015 software control interface

A software architecture, shown in Figure 5-28, illustrates the level of controls in
the software system. It indicates roles of each electrical component and the flow of data. A
detailed procedure is as the followings:

1. Point Grey 2D HD camera and Gocator 2380 laser scanner are triggered via
   Visual Studio

2. Both sensors are calibrated at a certain fixed resolution and scanning frequency

3. High-resolution 2D images are passed back to the communication interface via
   Gigabit Ethernet.

4. Cuttings moving speed is calculated by computer vision algorithms

5. Cuttings size distribution is generated by computer vision algorithms and data
   is stored for display

6. 2D profile depth data is passed back to the communication interface in the form of raw data points via Gigabit Ethernet

7. Measured speed is used to synchronize with 2D profile data for volume calculation and 3D profile reconstruction.

8. 3D profile reconstruction is performed either in real-time or off-line mode.

9. 3D profile data is stored.
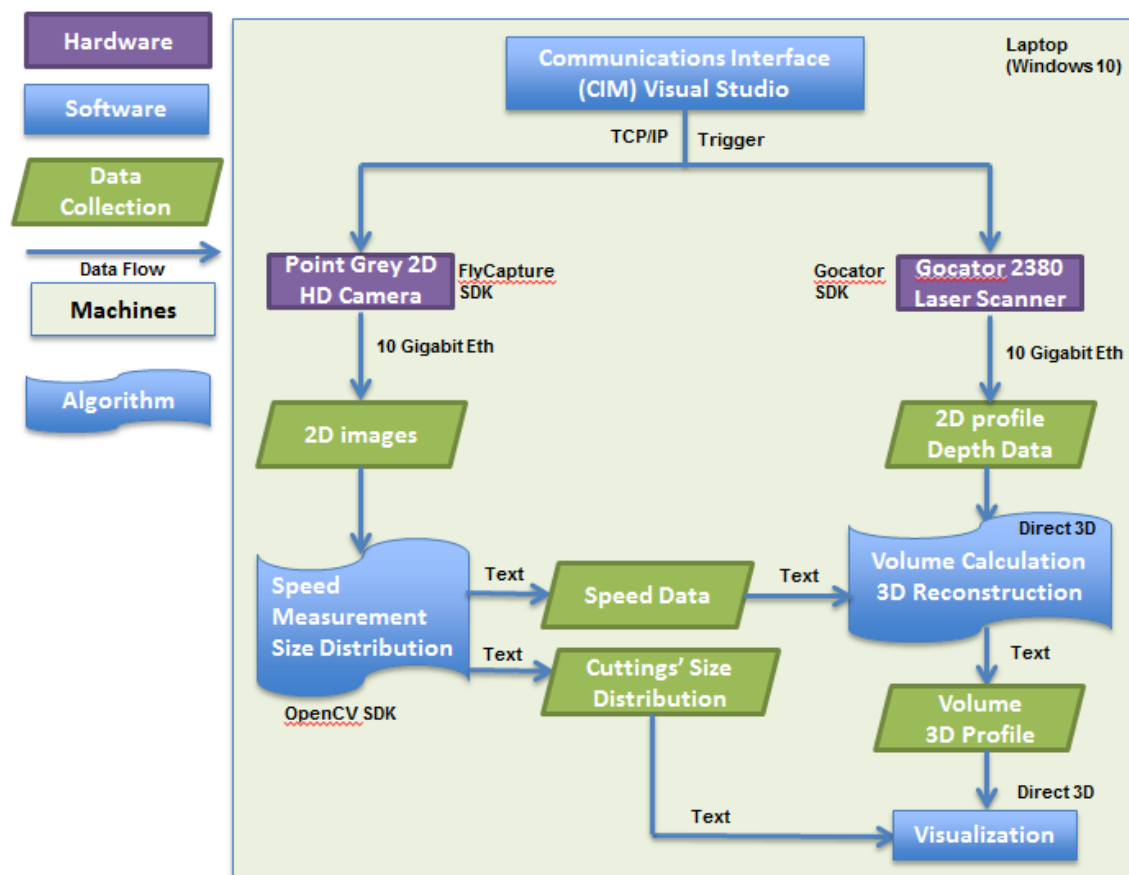
Figure 5-28: Software architecture

5.4 EXPERIMENT DESIGN

Section 5.4 presents a description how cuttings are measured against different scenarios in the laboratory environment. The measuring algorithms are based on computer vision system which has been explained in Chapter 3.

The objective of the experiment is to evaluate the proposed computer vision technique and generate an experimental threshold for void space correction when calculating cuttings volume. The experiment includes two parts: 1) uniform-shape objects testing and 2) real cuttings testing. The purpose to test uniform-shape objects is to validate the volume measurement against the detected moving speed, since the uniform shaped objects have either fixed void space ratio or no void space. Three uniform-shapes targets are ping-pong ball, aluminum bar, and aluminum rod as shown in Figure 5-29. The experiment procedure is listed below:

1. Adjust the tilting angle of the yellow ramp to 40 degrees.

2. Clear any cuttings left on the yellow ramp to make sure a clear scan.

3. Turn on the program and calibrate the laser scanner and 2D HD camera.

4. Place the ping-pong ball at the upper part of the yellow ramp at a fixed position (0.5 meters from the laser line along the ramp) to create some initial speed.

5. Record measured speed and calculated volume of the targets

6. Store 3D depth data in txt file format

7. Actual volume of the targets is calculated based on the physical dimensions.

8. Repeat steps 1-7 for another nine more times.

9. Repeat the procedure with different angles (45°, 50°, 60°, 70°, and 75°) yellow ramp that were selected to minimize the impact of both tumbling at high angles and static friction at lower angles.

10. Repeat the whole procedure with aluminum cube and aluminum rod.

Figure 5-29 a) Ping-pong ball (Sellercube 2016) radius = 40mm b) Aluminum bar (15mm x 30 mm x 70mm) c) Aluminum rod (OD= 25 mm, length = 100 mm)

Then for drillings cuttings testing, the sample used in this experiment were all from the same formation interval collected from the field. The shapes are random as shown in Figure 5-30 and size distribution of cuttings is relatively consistent. The cuttings have a composition of 70% shale and 30% sandstone. The distance between the sensors and the yellow ramp is kept constant at 1 meter. The frame rate of Point Grey Blackfly camera is set as 30 fps. The scanning frequency of Gocator 2380 laser scanner is set as 100 Hz. The experiment procedure is listed below:

1. Adjust the tilting angle of the yellow ramp to 40 degrees.
2. Clear any cuttings left on the yellow ramp to make sure a clear scan.
3. Prepare a certain amount of dry cuttings in the bucket.
4. Turn on the program and calibrate the laser scanner and 2D HD camera.
5. Pour down the cuttings at 20 cm above the top of the yellow ramp at a fixed position (0.5 meters from the laser line along the ramp) to create some initial speed.
6. Record measured speed and calculated volume of drilling cuttings
7. Store 3D depth data in txt file format
8. Collect all the experiment cuttings at the bottom of the yellow ramp.

9. Use a measuring cylinder to calculate the actual volume of cuttings.

10. Repeat the above steps 1-10 for nine different sets of cuttings from the same interval of drilling through homogeneous formation.

11. Repeat the procedure with different angles (45°, 50°, 60°, 70°, and 75°) yellow ramp that were selected to minimize the impact of both tumbling at high angles and static friction at lower angles.

Figure 5-30: Drilling cuttings sample.

Chapter 6 Results and Discussion

This chapter presents the experimental results and corresponding discussion. First, the experiment on testing uniform-shape objects is evaluated to analyze the accuracy of speed measurement and volume measurement. Second, drilling cuttings measurement result is evaluated and a void-space correction threshold is calculated based on the experimental results.

6.1 UNIFORM-SHAPE OBJECT TESTING

As discussed in Chapter 5, this unique computer vision system relies first on accurate speed measurement of the object and then on the resolution of the laser profile scanner. One method to test speed measurement is by using a conveyor belt. However, such equipment was not available in the laboratory.   To test the accuracy of the algorithm, spherical-shape ping-pong ball, aluminum bar, and aluminum rod are tested to compare the measured volume to actual volume.

The 2D laser profile scanner only generates depth data of the target's surface. Therefore, the space vertical below the top surface is also included in volume calculation. With known dimensions of the three uniform-shape objects, the over-calculated volume ratio can be calculated as followings:

$$\emptyset_{sphere} = \frac{\pi r^2 \times r - \frac{1}{2} \times \frac{4}{3}\pi r^3}{\frac{4}{3}\pi r^3} = 25\%$$

$$\emptyset_{cube} = 0\% \ (since \ the \ rectagular \ bar \ is \ sitting \ on \ the \ sliding \ ramp)$$

$$\emptyset_{rod} = \frac{2r \times L \times r - \frac{1}{2} \times \pi r^2 \times L}{\pi r^2 \times L} = 13.67\%$$

Then these ratios are applied to the uniform-shaped objects' measured volumes accordingly.

$$Corrected\ Measured\ Volume = \frac{Measured\ Volume}{1 + \emptyset}$$

The experimental results of the three uniform-shape objects are summarized in Table A-1, Table A-2, and Table A-3 of Appendix. The following Table 6-1 shows the calculated volume measurement error percentage.

Table 6-1: Volumetric measurement error percentage for uniform-shaped objects

	Ramp Angle					
	45°	50°	60°	70°	75°	Average
Sphere	0.97 %	2.65%	4.30%	0.08%	-1.09%	1.38%
Rectangular Bar	2.05%	0.62%	1.99%	3.21%	2.78%	2.13%
Rod	2.91%	3.74%	3.88%	0.72%	2.16%	2.68%

Based on the uniform-shape objects testing experiment, the average measurement error for the volume was less than 3%. The experiment was performed by varying the moving speed of the object. This demonstrated that the speed measurement algorithm and volume calculation are relatively reliable and accurate.

6.2 DRILLING CUTTINGS TESTING

In the previous experiment, it has been demonstrated that the proposed computer vision system is capable of tracking object's moving speed and measuring object's volume in the laboratory environment. However, compared to uniform-shaped objects, drilling cuttings have irregular shape and distribution, which makes it impossible to calculate a

void space threshold for a pile of moving cuttings. The void space threshold is critical for accurate volume estimation.

Different amounts of cuttings moved down the yellow ramp at various speed. Experimental result is presented in Table A-4. The following two figures plot over-calculated volume in percentage against sample volume and cuttings moving speed respectively. No obvious correlations have been spotted between cuttings moving speed, sample size, and the calculated volume. The over-calculated volume, as the void space below cuttings surface, distributed between 30% to 45%. An average volume fraction is calculated from Table A-4 as $\emptyset=37.18\%$. This is an experimental threshold which can be used to correct the volume measurement of dry cuttings in the laboratory environment.

$$Corrected\ Measured\ Volume = \frac{Measured\ Volume}{1 + 37.18\%}$$
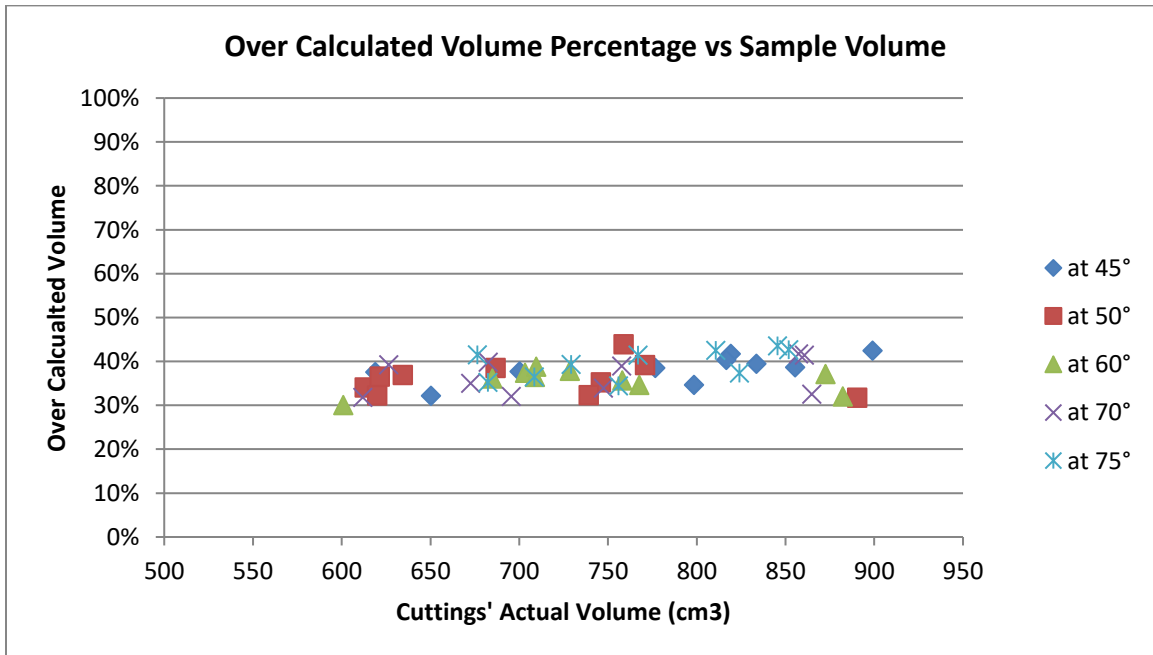
Figure 6-1: Over-calculated volume against cuttings actual volume

79
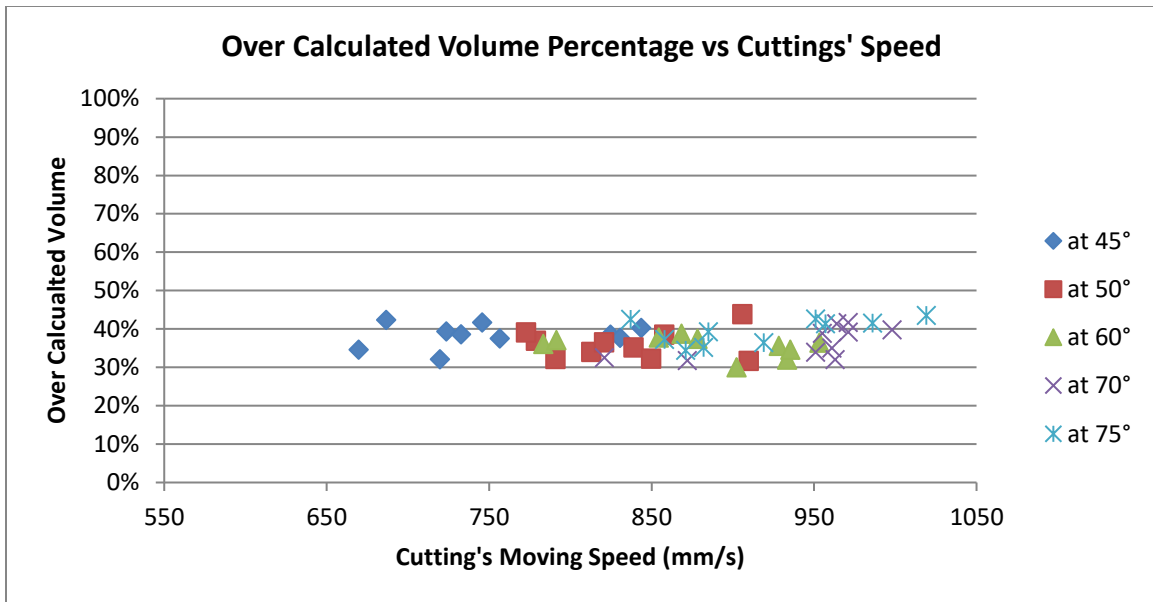
Figure 6-2: Over-calculated volume against cuttings moving speed.

This experimental calculated threshold is only good for dry cuttings testing in laboratory environment. On a drilling rig, cuttings are wet with the presence of drilling fluid, which will have a major impact on the packing ratio of the moving cuttings on the ramp. However, this number can be used as a reference value before a field testing. The computer vision system is strongly affected by ambient environment and the cuttings void fraction depends on several key drilling parameters. More details will be discussed for future work in Chapter 7.

Another factor influencing the void fraction ratio is the packing geometry for multi-layers of particles. For example, equal spheres have several packing possibilities: tetrahedral lattice, cubic lattice, cubic close packing, hexagonal close packing, etc. (Mathworld 2016). Figure 6-3 and Figure 6-4 are primitive cubic packing and body-centered packing respectively. The following calculations demonstrate how packing ratio affects volume measurement based on top surface geometry.
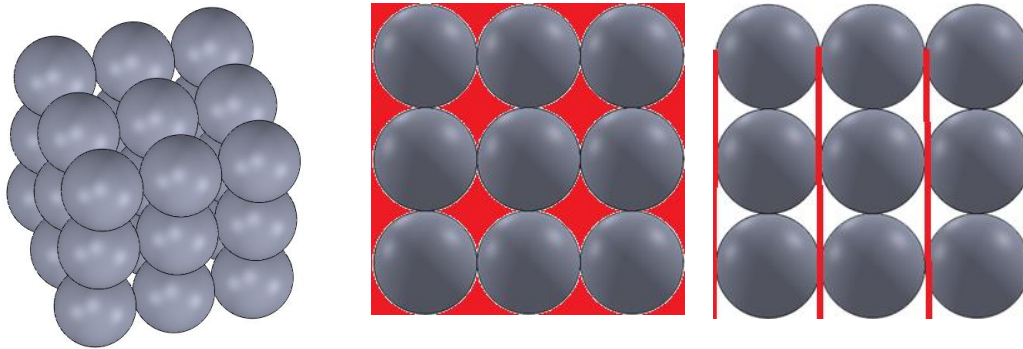
Figure 6-3: Primitive cubic packing. Perspective view (left), top view (middle), and side view (right)

For primitive cubic packing:

1. Actual solid volume $V_a = 27 \times \frac{4}{3} \times \pi \times r^3 = 36\pi r^3$

2. As laser sensor scans on the top surface, the red shaded area is viewed as void but the scanned profile will appear as nice cylinders. Because top layers covers the laser scan. The void space between red lines will be over measured as volume. Then the scanned volume is:

$$V_s = 9 \times \left(\pi r^2 \times 5r + \frac{2}{3}\pi r^3\right) = 51\pi r^3$$

3. The over-calculated volume ratio is:

$$\varnothing_p = \frac{51\pi r^3 - 36\pi r^3}{36\pi r^3} = 41.47\%$$
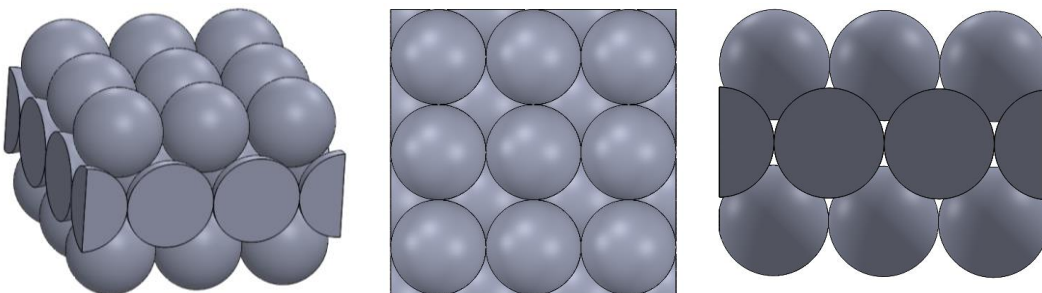
Figure 6-4: Body-centered cubic packing. Perspective view (left), top view (middle), and side view (right)

81

For body-centered cubic packing:

1. Actual solid volume $V_a = 27 \times \frac{4}{3} \times \pi \times r^3 = 36\pi r^3$

2. As the laser sensor scans the top surface, due to the packing geometry, the first two layers blocked all the space below. Based on some calculations, the scanned volume can be estimated as:

$$V_s = (6r)^2 \times \left(r + \sqrt{2}r\right) + 4.5 \times \frac{4}{3} \times \pi r^3 + 9 \times \left(\pi r^2 \times \sqrt{2}r + \frac{1}{2} \times \frac{4}{3}\pi r^3\right)$$

$$- \, 0.465741r^3 \times 4 \times 9 \approx 147.83r^3$$

3. The over-calculated volume ratio is:
$$\varnothing_p = \frac{147.83r^3 - 36\pi r^3}{36\pi r^3} = 30.71\ \%$$

As a result, it can be concluded that with different packing geometry, it affects how the laser scanner can scan the volume of target based on top surface profile. More experiments should be contact to derive a correlation between the over-calculated volume ratio and stacking geometry of measuring particles.

Chapter 7: Conclusions and Future Works

7.1 CONCLUSIONS

The primary objective of the present work was to develop an automated computer vision system which can be implemented on an oil rig for real-time monitoring of cuttings/cavings, return volume, size distribution, and 3D profile.

The current procedures for measuring cuttings either require human handling or lacks certain functionalities, such as 3D model reconstruction. With the fast development of 3D sensing technology during the last decade, various commercial 3D scanners are capable of volume measurement. After evaluating and testing some advanced 3D scanners, Gocator 2380 laser profile scanner was chosen for its high resolution ($\pm 1mm$), fast scanning speed, compact size, and large FOV. The trade-off for high resolution and fast scanning speed is that it only provides high frequency 2D profile data. Then, the next challenge was to measure how fast cuttings were sliding down the ramp. By applying a series of digital imaging processing techniques leveraging the OpenCV library, the cuttings moving speed and size distribution were estimated. Then the synchronization of input speed and 2D depth data enabled the volume of scanned target to be calculated. A 3D surface profile of the cuttings was also generated. To verify the accuracy of proposed system, uniform-shaped objects were tested and an error less than 3% for volumetric measurement was achieved. As cuttings sliding down the ramp, the top surface of cuttings covers some void space. By running the experiment at different speeds, an empirical volume correction factor was obtained.

Even though the algorithms were validated based on a lab setting, this work proposed a state-of-art non-intrusive computer visualization system to accurately evaluate

cuttings volume, size distribution, and surface profile. Future work is required to test and improve the vision processing techniques in the field where cuttings are coated with drilling fluid and illumination varies.

7.2 FUTURE WORKS

This work primarily focuses on designing a physical sensing system and computer vision algorithms to measure cuttings and cavings properties. It sets a foundation for establishing a comprehensive automated cuttings monitoring system to real-time supervise hole cleaning efficiency and wellbore stability. To expand this work, following recommendations should be considered in the future:

- **Shape characterizations and analysis** – as reviewed in Chapter 3, the shape of cavings gives the direction indication of rock failing mechanism. With the 3D model of reconstructed cuttings /caving surface, machine vision algorithms can be developed to analyze point cloud depth data and characterize the shapes of cavings based on length, width, thickness, and corner angle. Such algorithm will allow the system to automatically detect cavings and identify wellbore instability.

- **Field Trial** – as mentioned in Chapters 4 and 5, the speed tracking vision algorithm (background subtraction method) strongly depends on adjusting certain parameters for different lighting environment. Therefore, it is crucial to test this algorithm on a drilling rig under different lighting conditions.

- **Speed tracking improvement** - another image processing technique called Optical Flow (OpenCV 2016) should also be tested. This algorithm is based on feature matching and vector calculation which makes it less affected by the change in ambient lighting conditions.

- **Uniform-shaped objects stacking test** – as discussed in Chapter 6, when there are multi layers of objects, different packing geometries lead to different top surface geometry. The top surface profile dominates volume measurement. More experiment should be performed in the laboratory for uniform-shaped objects at different packing scenarios.

- **Cuttings size and shape model** – Different drill bits will generate different shapes of cuttings (as reviewed in Chapter 3). It is essential to design a model based on drill bit types to theoretically estimated cuttings void space ratio. Additionally, numerous 3D depth data should be collected in field trials in order to obtain an empirical ratio.

- **Cuttings bed thickness model** – based on the layers of cuttings on the ramp, the packing geometry various. Because of irregular shape of cuttings, it will be difficult to theoretically estimate void space ratio. On the other hand, a correlation between void space ratio and cuttings bed thickness can be investigated based on field trial data.

- **Explosion-proof enclosure** – according to Occupational Safety and Health Administration (OSHA) in Texas (OSHA 2016), shale shaker system area is considered a hazards working zone. Class I Division I explosion protection enclosure should be applied for all electronic devices for hydrocarbon drilling activities. Since current 3D scanners are not designed for such condition, a proper explosion-proof housing should be designed/purchased before field trial.

- **Cuttings transport model** – Chapter 4 reviews a number of cuttings transport models from the literature. In order to correlate measured cuttings volume with theoretical return volume, a comprehensive cuttings transport model should be established in the system. Drilling information, such as, fluid rheology, flow rate,

hole angle, etc., should be retrieved in real-time for cuttings traveling velocity estimation. Only with the assist of accurate cuttings transport model, the system can then relate detected cavings and cuttings size distribution to the formation depth.

- **Fine cuttings particles in drilling mud** – during drilling process, fine cuttings particles cannot be screened out by shale shaker system. The assessment of the difference between return mud weight and initial mud weight would be necessary for a full accounting of the cuttings. This calculation is complicated by other factors changing mud weight including: barite sag, hydrocarbon influx etc..

Appendix

Table A-1: Experimental results of Ping-pong ball

#	Angle (°)	Measured Speed (mm/s)	Measured Volume (mm3)	Actual Volume (mm3)	Over Calculated Percentage (%)	Corrected Measured Volume (mm3)	Error %
1	45	2394	347179	268083	29.50%	277742.8	3.60
2	45	2361	342394	268083	27.72%	273914.8	2.18
3	45	2270	329199	268083	22.80%	263358.8	-1.76
4	45	2386	346019	268083	29.07%	276814.8	3.26
5	45	2195	318324	268083	18.74%	254658.8	-5.01
6	45	2341	339494	268083	26.64%	271594.8	1.31
7	45	2313	335434	268083	25.12%	268346.8	0.10
8	45	2303	333984	268083	24.58%	267186.8	-0.33
9	45	2262	328039	268083	22.36%	262430.8	-2.11
10	45	2506	363336	268083	35.53%	290669.1	8.43
1	50	2591	336873	268083	25.66%	269498.4	0.53
2	50	2616	340123	268083	26.87%	272098.4	1.50
3	50	2677	348053	268083	29.83%	278442.4	3.86
4	50	2732	355203	268083	32.50%	284162.4	6.00
5	50	2645	343893	268083	28.28%	275114.4	2.62
6	50	2584	335963	268083	25.32%	268770.4	0.26
7	50	2666	346623	268083	29.30%	277298.4	3.44
8	50	2655	345193	268083	28.76%	276154.4	3.01
9	50	2669	347013	268083	29.44%	277610.4	3.55
10	50	2622	340903	268083	27.16%	272722.4	1.73
1	60	2739	342343	268083	27.70%	273874	2.16
2	60	2837	354593	268083	32.27%	283674	5.82
3	60	2812	351468	268083	31.10%	281174	4.88
4	60	2830	353718	268083	31.94%	282974	5.55
5	60	2897	362093	268083	35.07%	289674	8.05
6	60	2867	358343	268083	33.67%	286674	6.93
7	60	2719	339843	268083	26.77%	271874	1.41
8	60	2755	344343	268083	28.45%	275474	2.76
9	60	2785	348093	268083	29.85%	278474	3.88
10	60	2723	340343	268083	26.95%	272274	1.56
1	70	2920	335821	268083	25.27%	268656.5	0.21
2	70	3000	345021	268083	28.70%	276016.5	2.96
3	70	2854	328231	268083	22.44%	262584.5	-2.05

4	70	2870	330071	268083	23.12%	264056.5	-1.50
5	70	2961	340536	268083	27.03%	272428.5	1.62
6	70	2892	332601	268083	24.07%	266080.5	-0.75
7	70	2924	336281	268083	25.44%	269024.5	0.35
8	70	2903	333866	268083	24.54%	267092.5	-0.37
9	70	2949	339156	268083	26.51%	271324.5	1.21
10	70	2888	332141	268083	23.89%	265712.5	-0.88
1	75	3125	343760	268083	28.23%	275008.1	2.58
2	75	2951	324620	268083	21.09%	259696.1	-3.13
3	75	2944	323850	268083	20.80%	259080.1	-3.36
4	75	3059	336500	268083	25.52%	269200.1	0.42
5	75	2978	327590	268083	22.20%	262072.1	-2.24
6	75	2950	324510	268083	21.05%	259608.1	-3.16
7	75	3122	343430	268083	28.11%	274744.1	2.48
8	75	2959	325500	268083	21.42%	260400.1	-2.87
9	75	2970	326710	268083	21.87%	261368.1	-2.50
10	75	3066	337270	268083	25.81%	269816.1	0.65

Table A-2: Experimental results of aluminum rectangular bar

#	Angle (°)	Measured Speed (mm/s)	Measured Volume (mm3)	Actual Volume (mm3)	Over Calculated Percentage (%)	Error (%)
1	45	833.92	32236	31500	2.34	2.34
2	45	803.92	31076	31500	-1.34	-1.34
3	45	832.92	32197	31500	2.21	2.21
4	45	833.92	32236	31500	2.34	2.34
5	45	851.92	32932	31500	4.55	4.55
6	45	824.92	31888	31500	1.23	1.23
7	45	796.92	30806	31500	-2.20	-2.20
8	45	815.92	31540	31500	0.13	0.13
9	45	870.92	33666	31500	6.88	6.88
10	45	850.92	32893	31500	4.42	4.42
1	50	859.78	31798	31500	0.95	0.95
2	50	886.78	32797	31500	4.12	4.12
3	50	831.78	30762	31500	-2.34	-2.34
4	50	851.78	31502	31500	0.01	0.01
5	50	881.78	32612	31500	3.53	3.53
6	50	837.78	30984	31500	-1.64	-1.64
7	50	859.78	31798	31500	0.95	0.95
8	50	837.78	30984	31500	-1.64	-1.64
9	50	902.78	33388	31500	5.99	5.99
10	50	819.78	30319	31500	-3.75	-3.75
1	60	953.58	33047	31500	4.91	4.91
2	60	896.58	31072	31500	-1.36	-1.36
3	60	923.58	32008	31500	1.61	1.61
4	60	876.58	30379	31500	-3.56	-3.56
5	60	925.58	32077	31500	1.83	1.83
6	60	962.58	33359	31500	5.90	5.90
7	60	931.58	32285	31500	2.49	2.49
8	60	881.58	30552	31500	-3.01	-3.01
9	60	952.58	33013	31500	4.80	4.80
10	60	965.58	33463	31500	6.23	6.23
1	70	932.06	31556	31500	0.18	0.18
2	70	966.06	32707	31500	3.83	3.83
3	70	985.06	33350	31500	5.87	5.87
4	70	979.06	33147	31500	5.23	5.23
5	70	933.06	31590	31500	0.28	0.28
6	70	998.06	33790	31500	7.27	7.27

7	70	939.06	31793	31500		0.93	0.93
8	70	912.06	30879	31500		-1.97	-1.97
9	70	953.06	32267	31500		2.43	2.43
10	70	1005.06	34027	31500		8.02	8.02
1	75	972.03	33041	31500		4.89	4.89
2	75	993.03	33755	31500		7.16	7.16
3	75	1040.03	35353	31500		12.23	12.23
4	75	879.03	29880	31500		-5.14	-5.14
5	75	924.03	31410	31500		-0.29	-0.29
6	75	960.03	32633	31500		3.60	3.60
7	75	866.03	29438	31500		-6.55	-6.55
8	75	967.03	32871	31500		4.35	4.35
9	75	900.03	30594	31500		-2.88	-2.88
10	75	975.03	33143	31500		5.22	5.22

Table A-3: Experimental results of aluminum rod

#	Angle (°)	Measured Speed (mm/s)	Measured Volume (mm3)	Actual Volume (mm3)	Over Calculated Percentage (%)	Corrected Measured Volume (mm3)	Error %
1	45	2017	59138	49087	20.47%	52025.79	5.99
2	45	1995	58493	49087	19.16%	51458.33	4.83
3	45	2026	59402	49087	21.01%	52257.94	6.46
4	45	2026	59402	49087	21.01%	52257.94	6.46
5	45	1934	56704	49087	15.52%	49884.89	1.62
6	45	1923	56382	49087	14.86%	49601.16	1.05
7	45	1885	55267	49087	12.59%	48620.99	-0.95
8	45	1857	54447	49087	10.92%	47898.76	-2.42
9	45	1909	55971	49087	14.02%	49240.04	0.31
10	45	2012	58991	49087	20.18%	51896.82	5.72
1	50	1987	56522	49087	15.15%	49724.71	1.30
2	50	2058	58542	49087	19.26%	51501.74	4.92
3	50	1965	55896	49087	13.87%	49174.08	0.18
4	50	2109	59993	49087	22.22%	52778.2	7.52
5	50	2089	59424	49087	21.06%	52277.62	6.50
6	50	2030	57745	49087	17.64%	50800.94	3.49
7	50	1978	56266	49087	14.62%	49499.45	0.84
8	50	2074	58997	49087	20.19%	51902.19	5.73
9	50	1988	56551	49087	15.20%	49749.74	1.35
10	50	2070	58883	49087	19.96%	51802.08	5.53
1	60	2111	56620	49087	15.35%	49810.78	1.47
2	60	2176	58363	49087	18.90%	51344.43	4.60
3	60	2185	58605	49087	19.39%	51556.78	5.03
4	60	2220	59543	49087	21.30%	52382.59	6.71
5	60	2178	58417	49087	19.01%	51391.61	4.69
6	60	2149	57639	49087	17.42%	50707.37	3.30
7	60	2142	57451	49087	17.04%	50542.21	2.96
8	60	2235	59946	49087	22.12%	52736.51	7.43
9	60	2160	57934	49087	18.02%	50966.91	3.83
10	60	2054	55091	49087	12.23%	48465.88	-1.27
1	70	2281	57743	49087	17.63%	50798.65	3.49
2	70	2231	56477	49087	15.05%	49684.9	1.22
3	70	2234	56553	49087	15.21%	49751.72	1.35
4	70	2215	56072	49087	14.23%	49328.5	0.49
5	70	2238	56654	49087	15.41%	49840.82	1.53

6	70	2205	55819	49087	13.71%	49105.75	0.04
7	70	2165	54806	49087	11.65%	48214.75	-1.78
8	70	2155	54553	49087	11.13%	47992	-2.23
9	70	2322	58781	49087	19.75%	51711.92	5.35
10	70	2155	54553	49087	11.13%	47992	-2.23
1	75	2391	58690	49087	19.56%	51631.67	5.18
2	75	2345	57561	49087	17.26%	50638.46	3.16
3	75	2398	58862	49087	19.91%	51782.81	5.49
4	75	2223	54566	49087	11.16%	48004.3	-2.21
5	75	2326	57094	49087	16.31%	50228.22	2.32
6	75	2391	58690	49087	19.56%	51631.67	5.18
7	75	2243	55057	49087	12.16%	48436.13	-1.33
8	75	2333	57266	49087	16.66%	50379.36	2.63
9	75	2333	57266	49087	16.66%	50379.36	2.63
10	75	2339	57413	49087	16.96%	50508.91	2.90

Table A-4: Experimental results of drilling cuttings

#	Angle (°)	Measured Speed (mm/s)	Measured Volume (mm3)	Actual Volume (mm3)	Error
1	45	776.6026	1074652	798404	0.346
2	45	703.6026	1280135	898971	0.424
3	45	747.6026	1160855	819234	0.417
4	45	791.6026	859019.9	650280	0.321
5	45	769.6026	1075522	776550	0.385
6	45	812.6026	1145763	816652	0.403
7	45	697.6026	1162036	833598	0.394
8	45	840.6026	1185528	855359	0.386
9	45	831.6026	851054.9	618949	0.375
10	45	678.6026	964216.7	700230	0.377
1	50	902.777	821235.1	612862	0.34
2	50	802.777	951157.1	686756	0.385
3	50	765.777	1008647	746041	0.352
4	50	900.777	868422.4	634348	0.369
5	50	744.777	1172683	890420	0.317
6	50	733.777	848160.5	621363	0.365
7	50	904.777	819690.2	620038	0.322
8	50	805.777	1091815	758732	0.439
9	50	807.777	977935.1	739180	0.323
10	50	746.777	1072276	770867	0.391
1	60	905.3333	932064.5	684838	0.361
2	60	782.3333	1028055	758153	0.356
3	60	876.3333	966338.3	703303	0.374
4	60	811.3333	1164710	882356	0.32
5	60	890.3333	966769.1	708775	0.364
6	60	957.3333	1196261	872546	0.371
7	60	937.3333	984988.6	709646	0.388
8	60	882.3333	781095.9	600843	0.3
9	60	828.3333	1033297	767680	0.346
10	60	793.3333	1003881	728506	0.378
1	70	863	917972.9	695434	0.32
2	70	859	1000769	747400	0.339
3	70	1003	1052581	757798	0.389

4	70	963	907923.6	672536	0.35
5	70	838	806527.7	611933	0.318
6	70	910	1216849	860572	0.414
7	70	815	1214824	857321	0.417
8	70	971	872108.9	626515	0.392
9	70	824	954228.7	682567	0.398
10	70	940	1145824	864773	0.325
1	75	927	1131301	823963	0.373
2	75	871	922446.6	682283	0.352
3	75	1023	957070.6	676375	0.415
4	75	955	1015969	755929	0.344
5	75	921	1084361	766875	0.414
6	75	975	1213331	845527	0.435
7	75	830	966403.5	708507	0.364
8	75	866	1015841	729247	0.393
9	75	971	1214727	851842	0.426
10	75	980	1155182	810654	0.425

Bibliography

O.C.T.G. Procter Consultancy Ltd. 2000. *OCTG NS-17 ABC of Hole Cleaning.* Aberdeen, Scotland: O.C.T.G. Procter Consultancy Limited.

Ablard, Peter, Chris Bell, David Cook, Ivan Fornasier, Sachin Sharma, Kevin Fielding, Geroge Haines, Kevin McCarthy, and and etc. 2012. "The Expanding Role of Mud Logging." *Schlumberger Ooilfield Review.* https://www.slb.com/~/media/Files/resources/oilfield_review/ors12/spr12/or2012 spr03_mudlog.pdf.

Acuity. 2013. "AccuProfile 820 Laser Scanners User's Manual." July 30. http://www.foxcontrols.co.za/download/files/product_uploads/acuity-ap820-users-manual.pdf.

Acuity. 2012. "The AccuProfile 820." http://www.disensors.com/downloads/products/AccuProfile%20820%202D%20L aser%20Scanner_1160_79688.pdf.

Alex, Pham. 2009. *E3: Microsoft shows off gesture control technology for Xbox 360.* 6 1. http://latimesblogs.latimes.com/technology/2009/06/microsofte3.html.

API. 2009. *API Recommended Practice 13D - Rheology and hydraulics of oil-well drilling fluids.* Recommonded Practice, Washington: API.

Barnett, David, David Groth, and Jim McBee. 2004. "Cabling: The Complete Guide to Network Wiring." http://wolandblog.com/upload/Cabling_The_Complete_Guide_to_Network_Wiri ng.pdf.

Bruce Burr, Scott Dillard, Eric Drake, Brad Ivie, Craig Ivie, Roger Smith, Graham Watson. 2000. "On the Cutting Edge - Schlumberger Oildfield Review." https://www.slb.com/~/media/Files/resources/oilfield_review/ors00/aut00/p36_57 .pdf.

C. Aldea, A. W. Iyoho,M. Zamora. 2005. "Hole Cleaning: the Achilles' Heel of Drilling Performance? ." Houston, Texas: American Association of Drilling Engineers.

C.J. Hopkins, R.A. Leicksenring. 1995. "Reducing the Risk of Stuck Pipe in The Netherlands." Amsterdam: Society of Petroleum Engineers.

Carnegie Robotics . 2016. http://carnegierobotics.com/products/.

Chien, Sze-Foo. 1971. "ANNULAR VELOCITY FOR ROTARY DRILLING OPERATIONS ." In *lnt. J. Rock Mech. Min. Sci*, Vol. 9, pp. 403-416. Great Britain: Pergamon Press.

Chien, Sze-Foo. 1994. "Settling Velocity of Irregularly Shaped Particles." *SPE Drilling & Completion* (Society of Petroleum Engineers) 281 - 289.

Cranford, P.J., Muschenheim, D.K., Loder, J.W.,Gordon, D.C. Jr, Keizer, P.D., and Kranck, K.,. 1992. *Predicting the environmental impacts of drilling wastes on Georges Bank scallop populations.* ICES Benthos Ecology Working Group.

CREATIVE. 2016. *CREATIVE SENZ3D.* http://us.creative.com/p/web-cameras/creative-senz3d.

D. Kumar, S. Ansar2, S. Wang, J. YiMing, S. Ahmed, M. Povstyanova, and B. Tichelaar. 2012. "Real-time Wellbore Stability Analysis: An Observation from Cavings at Shale Shakers." Singapore.

David Fofi, Tadeusz Sliwa, Yvon Voisin. 2004. "A Comparative Survey on Invisible Structured Light." http://www.le2i.cnrs.fr/IMG/publications/fofi04a.pdf.

Edwards, Ian R. Lewis Howell. 2001. *Handbook of Raman Spectroscopy: From the Research Laboratory to the Process Line.* CRC Press.

Geng, Jason. 2011. "Structured-light 3D surface imaging: a tutorial." *Advances in Optics and Photonics* pp. 128-160.

Gerig, Guido. 2013. "Structured Lighting." http://www.sci.utah.edu/~gerig/CS6320-S2013/Materials/CS6320-CV-S2013-StructuredLight.pdf.

GRAVES, W.V. Andrew, and Matthew Dennis ROWE. 2013. Down hole cuttings analysis . US Patent WO 2013089683 A1. June 20.

GRAVES, W.V. Andrew, and Matthew Dennis ROWE. 2013. Down hole cuttings analysis. WO Patent WO 2013089683 A1. June 20.

Huffington Post Canada. 2014. "BP Oil Spill: Dolphins Plagued By Death, Disease Years After Rig Explosion." February 12. http://www.huffingtonpost.ca/2014/02/12/bp-oil-spill-dolphins_n_4774754.html.

IDS, Imaging Development Systems GmbH. 2014. *Ensenso N20 Stereo 3D camera.* https://en.ids-imaging.com/store/ensenso-n20.html.

IDS. 2012. *Obtaining Depth Information from Stereo Images - Whitepaper.* https://de.ids-imaging.com/whitepaper.html?file=tl_files/downloads/whitepaper/IDS_Whitepaper_3D_Stereo_Vision.pdf.

Indeed. 2016. *Mud Logger Salary in Texas.* http://www.indeed.com/salary/q-Mud-Logger-l-Texas.html.

IPIECA. 2009. "Drilling fluids and health risk management." *International Petroleum Industry Environmental Conservation Association.* http://www.ogp.org.uk/pubs/396.pdf.

Jacqueline, Arild Saasen (University of Stavanger) | Tor H. Omland (StatoilHydro ASA) | Sigbjorn Ekrene (Geoservices S.A.) | Jerome Brévière (Geoservices S.A.) | Eric Villard (Geoservices S.A.) | Nils Kaageson-Loe (M-I SWACO) | Ahmadi Tehrani (M-I SWACO) |. 2009. "Automatic Measurement of Drilling Fluid and Drill-Cuttings Properties." Florida: Society of Petroleum Engineers.

Karimi, (Weahtherford) Moji. 2013. "Drill-Cuttings Analysis for Real-Time Problem Diagnosis and Drilling Performance Optimization." Jakarta: Society of Petroleum Engineers.

Larsen, Thor Inge F. 1990. *A Study of the Critical Fluid Velocity in Cuttings Transport for Inclined Wellbores.* Tulsa: University of Tulsa.

LASE. 2013. "LaseBVC - Bulk Volume Conveyor." *Industriele Lasertechnik GmbH.* http://www.lase.de/en/products/mining-volume/bulk-volume-conveyor-belt.html.

Li, Larry. 2014. "Time-of-Flight Camera – An Introduction." http://www.ti.com/lit/wp/sloa190b/sloa190b.pdf.

LMI. 2016. *Gocator 3D Smart Sensor With Open Source SDK.* http://lmi3d.com/content/customize-your-gocator-open-source-sdk.

LMI, Technologies. 2016. "Gocator 2300 Series." http://downloads.lmi3d.com/system/files/Gocator/documents/Gocator%202300%20Series/DATASHEET_Gocator_2300_US_WEB.pdf.

M.R. Andersen, T. Jensen, P. Lisouski, A.K. Mortensen, M.K. Hansen,T. Gregersen and P. Ahrendt. 2012. *Kinect Depth Sensor Evaluation for Computer Vision Applications.* Department of Engineering – Electrical and Computer Engineering, Aarhus University.

Maire, Michael Randolph. 2009. *Contour Detection and Image Segmentation .* Thesis, California Institute of Technology.

Marana, A.N., J.P. Papa, Marcus V.D. Ferreira, Kazuo Miura, and Francisco Assis Cavalcante Torres. 2010. "An Intelligent System To Detect Drilling Problems Through Drilled-Cuttings-Return Analysis." New Orleans: Society of Petroleum Engineers.

Mathworld. 2016. "Sphere Packing." http://mathworld.wolfram.com/SpherePacking.html.

Mauro Dalla Mura, Manuel Aravecchia and Michele Zanin. 2012. "Outdoor 3D with Kinect:preliminary results in the granulometry of fluvial sediments." *3DOM 3D OPTICAL METROLOGY Technologies of Vision.* March 8th-9th. http://3dom.fbk.eu/repository/files/lc3d/DallaMura_etal_lowcost3d-2012-Trento.pdf.

Michael Brading, Kenneth Salsman,Manjunath Somayaji,Brian Dipert,Tim Droz,Daniël Van Nieuwenhove,Pedro Gelabert. 2016. "3-D Sensors Bring Depth Discernment to Embedded Vision Designs." *Embedded Vision Alliance.* http://www.embedded-vision.com/platinum-members/embedded-vision-alliance/embedded-vision-training/documents/pages/3d-sensors-depth-discernment.

Microsoft. 2016. https://developer.microsoft.com/en-us/windows/kinect/develop.

Microsoft. 2016. *Classic DirectX Graphics.* https://msdn.microsoft.com/en-us/library/windows/desktop/hh309465(v=vs.85).aspx.

Microsoft. 2010. *Kinect for Windows Sensor Components and Specifications.* https://msdn.microsoft.com/en-us/library/jj131033.aspx?f=255&MSPPError=-2147217396.

Moore, L.P. 1974. In *Drilling Practices Manual*, Chap. 8. Tulsa: Petroleum Publishing Co.

Morton-Thompson, Diana, and Arnold M. Woods. 1993. "Mtds 10 - Development Geology Reference Manual." AAPG.

National Instruments. 2012. *Parts of a Stereo Vision System.* http://zone.ni.com/reference/en-XX/help/372916M-01/nivisionconceptsdita/guid-cb42607e-f256-40f5-ab6e-28ec3a33bcda/.

Omland, Tor Henry, Knut Taugbol, Terje Jorgensen, Frode Reinholt, and Per Amund Amundsen | Hans Erik Foss Amundsen et al. 2007. "Improved Drilling Process Control Through Continuous Particle and Cuttings Monitoring." Houston: Society of Petroleum Engineers.

OpenCV. 2016. "OPENCV-OPEN SOURCE COMPUTER VISION." http://opencv.org/.

OSHA. 2016. https://www.osha.gov.

Pietro Zanuttigh · Giulio Marin, Carlo Dal Mutto · Fabio Dominio, Ludovico Minto ·
    Guido Maria Cortelazzo. 2016. *Time-of-Flight and Structured Light Structured
    Light Structured Light.* Switzerland: Springer International Publishing.

Point Grey. 2016. *Bumblebee2 1394a.* https://www.ptgrey.com/bumblebee2-firewire-
    stereo-vision-camera-systems.

PointGrey. 2015. *Blackfly 2.3 MP Color GigE PoE (Sony Pregius IMX249).*
    https://www.ptgrey.com/blackfly-23-mp-color-gige-poe-sony-pregius-imx249.

PointGrey. 2016. "FlyCapture SDK." https://www.ptgrey.com/flycapture-sdk.

RIGEL. 2010. "2D laser Scanner LMS-Q20."
    http://www.riegl.com/uploads/tx_pxpriegldownloads/10_DataSheet_LMS-
    Q20_28-07-2010.pdf.

Rubiandini, Rudi. 1999. "Equation for Estimating Mud Minimum Rate for Cuttings
    Transport in an Inclined-Until-Horizontal Well." Abu Dhabi: Society of
    Petroleum Engineers.

Schlumberger. 2015. "CLEAR Hole Cleaning and Wellbore Risk Reduction Service."
    http://www.slb.com/~/media/Files/geoservices/product_sheets/clear_ps.pdf.

Sellercube. 2016. *Sellercube.*
    http://img.sellercube.com/UploadFile/6/SKU032820/20120515150716945.JPG.

SICK. 2015. "Bulkscan LMS511."
    https://www.sick.com/media/dox/3/13/613/Product_information_Bulkscan_LMS5
    11_en_IM0045613.PDF.

SICK. 2013. "LMS400 Laser measurement sensor."
    https://www.sick.com/media/dox/8/98/698/Operating_instructions_LMS400_Lase
    r_measurement_sensor_en_IM0010698.PDF.

SICK. 2012. "LMS400-2000 Data Sheet."
    https://www.sick.com/media/pdf/0/50/350/dataSheet_LMS400-
    2000_1041725_en.pdf.

SMITH, Adrian, E. 2012. SYSTEM AND METHOD FOR IMPROVED CUTTINGS MEASUREMENTS. WO Patent WO/2013/105930 . September 1.

Tobenna, Unegbu Celestine. 2010. *Hole Cleaning and Hydraulics* . Thesis, Stavanger: University of Stavanger.

Walz. 2014. "Walz Load Scanner (WLS)." *Load Scanner.* https://www.walzscale.com/store/show/title/load-scanner-details.

Wiersberg, Thomas. 2009. "Online Gas Monitoring of Drilling Mud (OLGA)." *International Continental Scientific Drilling Program (ICDP).* Accessed 2016. http://www-icdp.icdp-online.org/front_content.php?idcat=1704.

Zeidler, Udo H. 1972. *An Experimental Analysis of the Transport of Drilled Particles.* Thesis, Houston: Rice University.

Zennaro, Simone. 2014. *Evaluation of Microsoft Kinect 360 and Microsoft Kinect One for robotics and computer vision applications* . Thesis, UNIVERSITÀ DEGLI STUDI DI PADOVA DIPARTIMENTO DI INGEGNERIA DELL'INFORMAZIONE .